View metadata, citation and similar papers at core.ac.uk

brought to you by CORE

provided by CERN Document Server

arXiv:astro-ph/0609458 v1 15 Sep 2006

A Large, Uniform Sample of X-ray Emitting AGN from the ROSAT All-Sky and Sloan Digital Sky Surveys: the Data Release 5 Sample

Scott F. Anderson[1], Bruce Margon[2], Wolfgang Voges[3], Richard M. Plotkin[1], David Syphers[1], Daryl Haggard[1], Matthew J. Collinge[4], Jillian Meyer[1], Michael A. Strauss[4], Marcel A. Agüeros[1], Patrick B. Hall[5], L. Homer[1], Željko Ivezić[1], Gordon T. Richards[6], Michael W. Richmond[7], Donald P. Schneider[8], Gregory Stinson[1], Daniel E. Vanden Berk[8], Donald G. York[9]

anderson@astro.washington.edu, margon@stsci.edu, wvoges@mpe.mpg.de, plotkin@astro.washington.edu

ABSTRACT

We describe further results of a program aimed to yield $\sim 10^4$ fully characterized optical identifications of ROSAT X-ray sources. Our program employs X-ray data from the ROSAT All-Sky Survey (RASS), and both optical imaging and spectroscopic data from the Sloan Digital Sky Survey (SDSS). RASS/SDSS data from 5740 deg^2 of sky spectroscopically covered in SDSS Data Release 5 (DR5) provide an expanded catalog of 7000 confirmed quasars and other AGN that are probable RASS identifications. Again in our expanded catalog, the identifications as X-ray sources are statistically secure, with only a few percent of the SDSS AGN likely to be randomly superposed on unrelated RASS X-ray sources. Most identifications continue to be quasars and Seyfert 1s with $15 < m < 21$ and $0.01 < z < 4$; but the total sample size has grown to include very substantial numbers of even quite rare AGN, e.g., now including several hundreds of candidate X-ray emitting BL Lacs and narrow-line Seyfert 1 galaxies. In addition to exploring rare subpopulations, such a large total sample may be useful when considering correlations between the X-ray and the optical, and may also serve as a resource list from which to select the "best" object (e.g., X-ray brightest AGN of a certain subclass, at a preferred redshift or luminosity) for follow-on X-ray spectral or alternate detailed studies.

Subject headings: catalogs — surveys — quasars: general — quasars: individual — X-rays

[1]University of Washington, Department of Astronomy, Box 351580, Seattle, WA 98195

[2]Space Science Telescope Institute, 3700 San Martin Drive, Baltimore, MD, 21218

[3]Max Planck-Institute für extraterrestrische Physik, Geissenbachstr. 1, D-85741 Garching, Germany

[4]Princeton University Observatory, Princeton, NJ 08544

[5]Department of Physics & Astronomy, York University, 4700 Keele St., Toronto, ON, M3J 1P3, Canada

[6]Department of Physics and Astronomy, The Johns Hopkins University, 3400 North Charles Street, Baltimore, MD 21218-2686

[7]Department of Physics, Rochester Institute of Technology, Rochester, NY 14623-5603

[8]Department of Astronomy and Astrophysics, The Pennsylvania State University, University Park, PA 16802

[9]Astronomy and Astrophysics Center, University of Chicago, 5640 South Ellis Avenue, Chicago, IL 60637

1. Introduction

The premier X-ray imaging survey of the astronomical sky is the ROSAT All-Sky Survey (hereafter RASS; Voges et al. 1999, 2000). In the 1990s, RASS surveyed most of the celestial sphere in the $0.1-2.4$ keV range with the Position Sensitive Proportional Counter (PSPC; Pfeffermann et al. 1988) to a typical limiting sensitivity of $\sim 10^{-13}$ erg cm^{-2} s^{-1}, cataloging more than 10^5 X-ray sources in the RASS Bright and Faint Source Catalogs.

With RASS's typical X-ray positional uncertainty of order $\sim 10-30''$, the effort involved in optically identifying a large fraction of the cataloged abundant RASS sources may appear daunting; and yet, several large-scale identification efforts are currently making substantial progress. Thousands of optical identifications for RASS sources are now suggested, albeit with various levels of identification confidence on the nature of the counterparts, ranging from: statistical cross-correlations with Schmidt photographic plate images (e.g., see radio/optical/X-ray matches cataloged in Flesch and Hardcastle 2004); to optical spectral identification estimates from low spectral-resolution photographic Schmidt objective prism plates (e.g., see Zickgraf et al. 2003; Mickaelian et al. 2006); to digital optical photometry and multi-object spectrophotometry (e.g., see RASS Bright and Faint Source Catalog identifications in Anderson et al. 2003).

For comparison to such recent RASS efforts involving thousands of suggested optical identifications each, it may be recalled that the most complete optical identification effort at similar depth from *Einstein* X-ray data was the Extended Medium Sensitivity Survey (EMSS; e.g., Gioia et al. 1984, Stocke et al. 1991). Quasars/AGN were the predominant class in the EMSS, accounting for about half of the ~ 800 *Einstein* identifications. Although the EMSS total of ~ 400 AGN identifications is quite large in aggregate, certain subsets are critically small when subdivided; for example, although the EMSS provided fundamental insights into BL Lac evolution (Morris et al. 1991), the entire EMSS sample included only $\sim$40 BL Lacs.

In order to substantively expand on such earlier *Einstein* programs, current efforts should provide samples significantly exceeding $\sim 10^3$ spectroscopically secure optical identifications. Our approach, detailed previously in Anderson et al. 2003 (hereafter, Paper 1), relies on the very good sensitivity match between AGN detectable in X-rays with RASS and AGN accessible to good quality optical spectra with the Sloan Digital Sky Survey (SDSS; York et al. 2000). Our ultimate aim has been the cataloging and characterization of $\sim 10^4$ X-ray identifications; the AGN in this sample are not only statistically secure in their identifications as X-ray sources, but are also accompanied by high quality and uniform data in the X-ray from RASS and in the optical (both photometry and spectroscopy) from SDSS.

In section 2, we briefly review relevant aspects of the SDSS data, and the selection and confirmation of candidate AGN optical counterparts from SDSS; detailed descriptions of these aspects, and a much more complete set of references, may be found in Paper 1. In section 3, we present results from our RASS/SDSS program for 5740 deg^2 of sky (about $4\times$ the area coverage considered in Paper 1), providing an updated and expanded catalog of X-ray and optical properties of 7000 likely SDSS AGN identifications for RASS X-ray sources. In sections 3-4, we discuss some AGN subclasses of special interest, including more than 260 X-ray emitting BL Lac candidates, and 770 candidate X-ray emitting narrow-line Seyfert 1s and related quasars. Section 5 discusses the reliability of the identifications and some ensemble properties of the expanded sample. Section 6 provides an updated example optical/X-ray correlation study. A short summary is provided in Section 7.

2. Selected Aspects of SDSS Relevant to RASS Identifications

The SDSS is creating an optical digital imaging and spectroscopic database of a large portion of the celestial sphere, primarily in a region approaching $\sim 10^4$ deg^2 centered on the north Galactic polar cap. The optical data are obtained by a dedicated 2.5m telescope, located at Apache Point Observatory, New Mexico, equipped with a large-format mosaic camera that can image $\sim 10^2$ deg^2 in 5 colors (u, g, r, i, z) in a single night, as well as a multifiber spectrograph which obtains the spectra of 640 objects within a 7 deg^2 field simultaneously. The imaging database is used to select objects for the SDSS spectroscopic survey, which includes $(\lambda/\Delta\lambda \sim 1800)$ spectrophotometry covering a broad (3800-9200Å) wavelength range for 10^6 galaxies, 10^5 quasars, and 10^5 stars. Details on SDSS hardware, software, astrometric, photometric, and spectral data may be found in a variety of papers, including Fukugita et al. (1996), Gunn et al. (1998), Lupton et al. (1999), York et al. (2000), Hogg et al. (2001), Stoughton et al. (2002), Smith et al. (2002), Pier et al. (2003), Ivezić et al. (2004), Gunn et al. (2006), and Tucker et al. (2006). A description of the previous SDSS Public Data Release (DR4) is given by Adelman-McCarthy et al. (2006).

The depths of RASS and SDSS are well-matched. For example, quasars and BL Lacs are known to have extreme X-ray to optical flux ratios of order $log\ (f_x/f_{opt}) \sim 1.0 - 1.5$ (Stocke et al. 1991); so even unusually faint RASS optical counterparts will have magnitudes brighter than $m < 20 - 21$. The SDSS imaging survey at this depth provides accurate colors and magnitudes for nearly all RASS counterparts, and SDSS multi-object followup spectroscopy also typically yields excellent quality data. The RASS/SDSS area is also covered by the NVSS and/or FIRST 20 cm radio surveys (Condon et al. 1998; Becker, White & Helfand 1995), providing radio information for nearly all RASS/SDSS objects.

A detailed description of the SDSS "target selection pipeline" (Stoughton et al. 2002) algorithms applicable to RASS sources is provided in our Paper 1, so here we provide an abbreviated summary. Optical objects in the SDSS photometric catalogs are automatically cross-correlated with X-ray sources in the RASS Bright and Faint Source catalogs, and those SDSS optical objects within $1'$ of the X-ray source positions are initially flagged as potential positional matches to be considered further. Due to limitations on the number of spare SDSS fibers available for ROSAT identifications, and a $55''$ restriction on the minimum separation of adjacent fibers, we especially favor confirming optical spectroscopy of a single, high-priority SDSS candidate counterpart within $27.5''$ of the RASS X-ray position for each of the $\sim 10^4$ highest-significance RASS sources (X-ray detection likelihood ≥ 10) that lie within the joint RASS/SDSS sky coverage. SDSS spectroscopic limits for RASS candidate counterparts are approximately in the range $15 < m < 20.5$, where m refers here to g, or r, or i passbands.

Each SDSS optical object imaged in a RASS error circle is assigned to a graded (A,B,C,D,E) priority bin for follow-on SDSS optical spectroscopy. The priority bins are based on typical ratios of X-ray to optical flux for known subclasses of X-ray emitters, with SDSS optical magnitudes, colors, and image morphology, as well as FIRST radio data, serving as indicators of the likely object class during spectroscopic target-selection. The 'ROSAT_A' and 'ROSAT_B' (two highest priority) categories are specifically aimed at AGN, and encompass about 92% of the identifications presented here. These two categories are also highly efficient, with 85% of all targeted 'ROSAT_A' and 'ROSAT_B' objects returning spectra of AGN. 'ROSAT_A' objects are triple positional coincidences of a RASS X-ray source, an SDSS optical object, and a FIRST radio source, especially aimed at BL Lacs (and other X-ray/radio-emitting quasars). 'ROSAT_B' is assigned to SDSS objects having unusual optical colors indicative of AGN/quasars (Richards et al. 2002); UV excess and more sophisticated multicolor approaches are consulted, e.g., see Figure 1. The reader is referred to Paper 1 for details on the other ROSAT target selection categories.

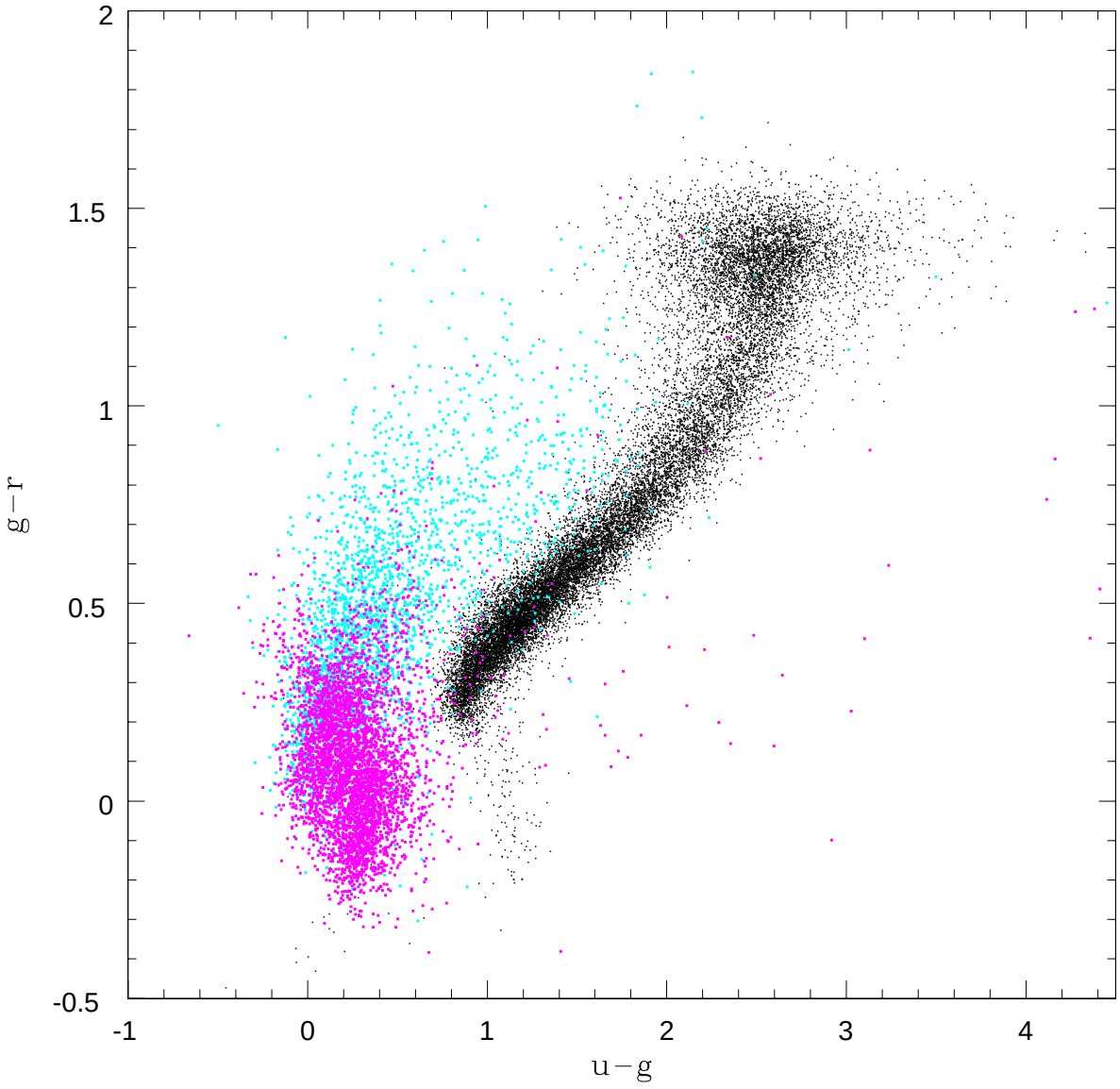

Fig. 1.— Optical SDSS colors of 7000 spectroscopically-confirmed quasars and other X-ray emitting AGN in our updated sample are overplotted for comparison on the locus of 10,000 anonymous SDSS stellar objects (black points). The *magenta* points show SDSS colors of quasi-stellar X-ray identifications that are unresolved in SDSS images, while *cyan* points show colors of AGN morphologically resolved in SDSS. Note the good color separation of the large majority of the confirmed quasar/AGN identifications.

Additionally, SDSS objects that are part of the main optical spectroscopic surveys of 10^6 galaxies and 10^5 quasars are assigned their spectroscopic fibers first, even before the SDSS/RASS target selection algorithms (making use of spare fibers) come into play. As a bonus to this identification program, SDSS spectra are thus available for the vast majority of such "tiled targets" (Blanton et al. 2003) falling fortuitously in RASS error circles; these include most galaxies to Petrosian $r < 17.77$, SDSS objects to $i < 19.1$ with quasar colors, and FIRST radio sources with optical PSF-morphology to $i < 19.1$. On the other hand, a galaxy targeted as part of the SDSS galaxy redshift-survey sample, and merely falling by chance near a RASS error circle, may sometimes eliminate a desired ROSAT target from any chance of receiving a spectroscopic fiber.

Thus, our expanded RASS/SDSS catalog is not a "complete" sample, though in practice we expect the catalog may eventually prove to be reasonably complete for most classes of X-ray emitting quasars and AGN with $15 < m < 19$. For these objects, quasar target selection completeness is confirmed to be high (Vanden Berk et al. 2005), and these may be selected for SDSS spectra by either spare-fiber ROSAT or tiled-fiber quasar target selection categories.

3. Expanded Catalog of 7000 X-ray Emitting AGN From RASS/SDSS

The expanded catalog of RASS/SDSS identifications is presented in this section. The emphasis in this installment of the RASS/SDSS catalog is on a set of 7000 X-ray emitting quasars/AGN. About 1200 of these constituted our original installment of the RASS/SDSS AGN catalog presented in Paper 1. For the full sample of 7000 AGN, the identifications are statistically secure, as discussed in §5.

We have examined an early version of the Data Release 5 (DR5) database and identified 15,129 SDSS spectra that fall within $1'$ of a RASS source. All of these spectra have been examined by a variety of methods, both algorithmic and visual, to search for plausible AGN identifications for the corresponding RASS X-ray sources. Our examination of the SDSS spectra taken within RASS error circles emphasizes searching especially for the following sets of AGN: (i) classic AGN/quasars with strong, broad emission lines; (ii) AGN with narrower line components; and, (iii) BL Lacs with weak or absent spectral features.

3.1. Quasars and Other AGN with Strong, Broad Permitted Lines

In Tables 1 and 2, we present an updated catalog of spectroscopically confirmed RASS/SDSS quasars and closely-related AGN having strong, broad permitted emission lines. All are in SDSS DR5 and have optical positions within $1'$ of RASS X-ray sources. Sample versions of Tables 1 and 2, listing only the first five entries, are included within this paper; the full tables are available electronically from the journal. We present the entire updated RASS/SDSS AGN catalog, including both new objects and those presented previously in Paper 1 (or elsewhere in the literature). Paper 1 included optical data from very early-on in the SDSS program (e.g., extending back to the "Early Data Release" before SDSS photometric calibrations were complete; Stoughton et al. 2002), so here we catalog all counterparts with their uniform SDSS DR5 photometric and spectroscopic parameters.

Included under the category of "broad-line" quasars, are RASS/SDSS objects whose spectra show characteristic strong optical emission lines of AGN, with broad permitted emission having velocity width in excess of 1000 km s^{-1} FWHM; the latter value is also that used in the DR3 quasar catalog of Schneider et al. (2005), and is close to the value of 1200 km s^{-1} that separates a bimodal line-width distribution seen in SDSS

Seyfert galaxies (Hao et al. 2005). In order to identify such broad-lined quasars, we first considered those spectra in which the SDSS spectroscopic 1D pipeline software (Stoughton et al. 2002) returned a best-fit Gaussian FWHM exceeding 1000 km s^{-1} for any of the following emission lines: Lyα, NV 1240, SiIV 1400 (blend), CIV 1549, CIII] 1909, MgII 2800, Hγ, Hβ, or Hα. Of the 15,129 SDSS DR5 spectra taken in RASS error circles, 7220 spectra appeared to satisfy this initial pipeline-based emission line-width criteria within the DR5 database. An additional 17 spectra were found in a subsequent by-eye examination (discussed in section 3.2) that are also clearly predominantly broad-lined AGN, but which failed the algorithmic cut discussed above based on spectroscopic pipeline measures; for example, this group includes some broad absorption line QSOs (BALQSOs), some cases with spectral reduction problems, etc.

We visually re-examined all 7237 spectra to confirm their nature, as well as to verify the pipeline redshifts. Among these, 6582 were visually confirmed to indeed be spectra of broad-line quasars, with only 9 requiring significant redshift corrections to the pipeline estimates. From the surviving list of 6582 confirmed broad-line AGN spectra, there are 6224 distinct objects; that is, about 5% of these AGN have more than one SDSS spectrum available in DR5. Although the line-width selection in this paper is based almost entirely on SDSS pipeline Gaussian-fit measures, 99% of the AGNs cataloged in Paper 1 (where classifications were based on manual line measures) are also recovered in this paper; the substantial recovery fraction is not a surprise of course, but worthy of verification given our far heavier reliance in the current paper on SDSS pipeline spectroscopic measures. Note also that we avoid any luminosity cuts, and so Tables 1 and 2 include not just most classic quasars and Sy 1s, but also many Sy 1.5s to Sy 1.9s, and even many rare objects such as narrow lined Seyfert 1s (NLS1s).

All AGN have confirming, high-quality SDSS optical spectra and imaging, uniformly reduced as part of DR5. See Figure 2 for representative examples of their SDSS spectra.

Following our format in Paper 1, Table 1 includes mainly empirical characteristics of the 6224 X-ray-emitting RASS/SDSS broad-line quasar/AGN counterparts, while Table 2 provides mainly derived information. Table 1 is ordered according to the RA (J2000) of the RASS X-ray source; the *1st column* lists the X-ray position, using RA/Dec nomenclature. The *2nd column* provides the optical position/nomenclature (J2000) of the suggested SDSS quasar/AGN counterpart. The *3rd through 7th columns* provide uniform DR5 optical PSF photometry in the 5 SDSS passbands (e.g., Fukugita et al. 1996) in the *asinh* AB system (Lupton, Gunn, & Szalay 1999). The *8th column* provides the value of the SDSS imaging morphology parameter: type=6 indicates stellar/unresolved optical morphology, while type=3 indicates an extended/resolved (i.e., galaxy) morphology. The *9th column* provides the redshift measured from SDSS spectra. The remaining columns of Table 1 emphasize empirical X-ray data from the RASS catalogs (e.g., see Voges et al. 1999, 2000). The *10th column* provides the RASS X-ray source count rate (counts s^{-1}) in the 0.1-2.4 keV broadband, corrected for vignetting. The *11th column* gives the RASS exposure time in seconds. The *12th and 13th columns* provide X-ray hardness ratios. The *14th column* is the X-ray source detection likelihood. The *15th column* gives the observed X-ray flux in the 0.1-2.4 keV band; we used the PIMMS (Portable, Interactive, Multi-Mission Simulator) software to convert RASS count rates into X-ray fluxes, assuming a power-law X-ray spectrum with energy index $\alpha_x = 1.5$, typical of low redshift quasars in the RASS PSPC bandpass (e.g., see Schartel et al. 1996).

In Table 2, we present further catalog information on the 6224 broad line RASS/SDSS AGN, emphasizing derived quantities. For cross reference to Table 1, we repeat in the *1st column* and *2nd column*, respectively, the RASS X-ray source and optical counterpart name/position. The *3rd column* provides the *g*-band PSF magnitude but here extinction corrected according to the reddening maps of Schlegel, Finkbeiner, & Davis (1998). The *4th column* repeats the SDSS spectroscopic redshift. The *5th column* is the X-ray flux

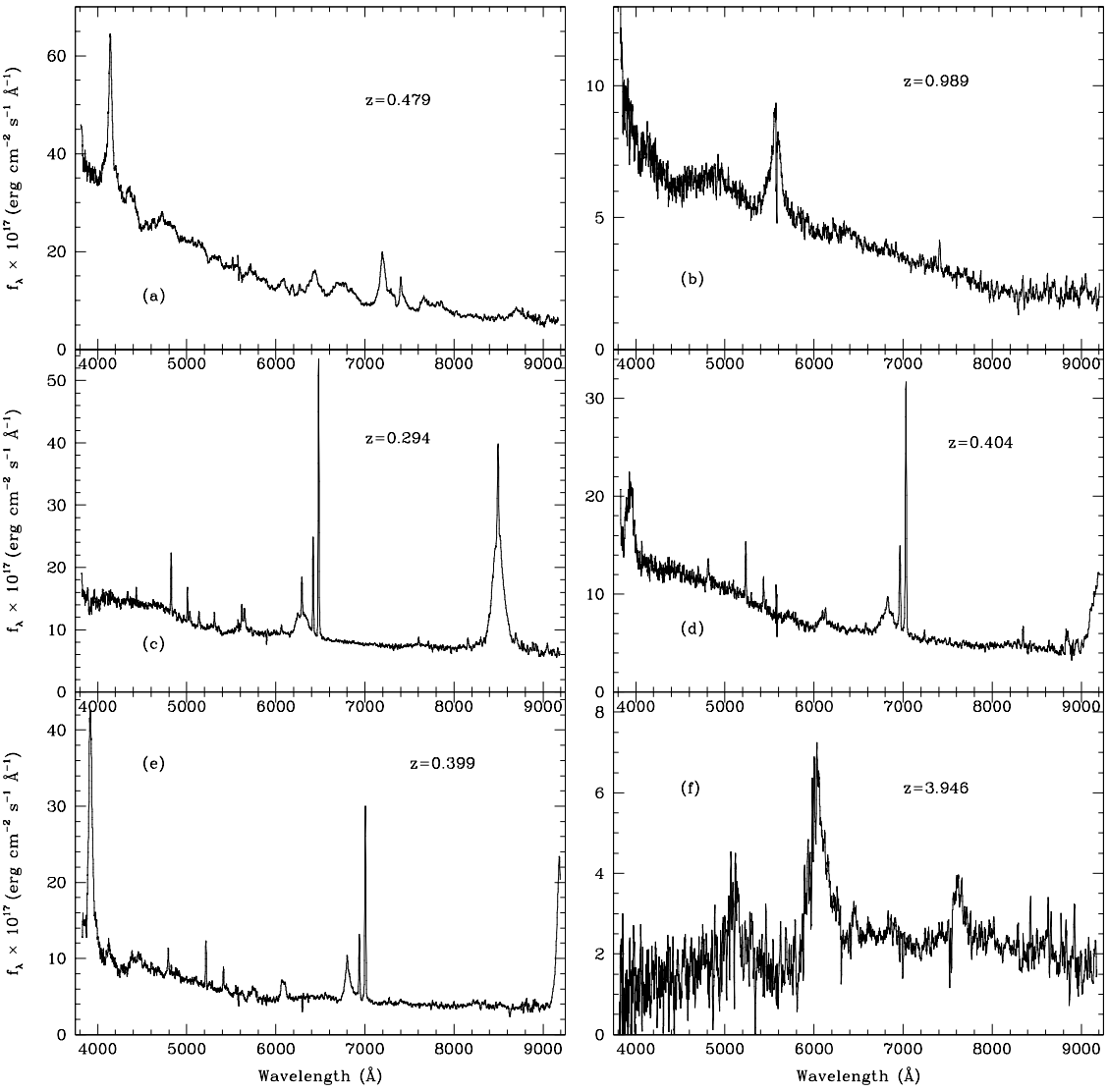

Fig. 2.— Representative SDSS optical spectra for RASS/SDSS X-ray emitting quasars/AGN with broad permitted emission lines, as discussed in section 3.1. Shown (a-e) are spectra smoothed with a 7 point boxcar for the first 5 objects listed in Tables 1-2, along with a high-redshift case (f) reflecting the very broad range of redshifts sampled. All 6224 broad line AGN cataloged have similar high-quality SDSS spectroscopy. (a) SDSS J000011.96+000225.3; (b) SDSS J000024.02+152005.4; (c) SDSS J000102.18−102326.9; (d) SDSS J000116.00+141123.0; (e) SDSS J000132.83+145608.0; (f) SDSS J081009.95+384757.0.

(units of 10^{-13} erg s^{-1} cm^{-2}) in the 0.1-2.4 keV band, now corrected for absorption within the Galaxy, with X-ray absorbing columns estimated using the N_H column density measures of the Stark et al. (1992) 21cm maps. The *6th, 7th, and 8th columns* give the logarithms of, respectively, inferred broadband (0.1-2.4 kev) X-ray luminosity (units of erg s^{-1}), UV/optical monochromatic luminosity (cgs units of erg s^{-1} Hz^{-1}) at a frequency corresponding to rest frame 2500 Å , and monochromatic X-ray luminosity (cgs) at 2 kev; we adopt values of H_0=70 km s^{-1} Mpc^{-1}, $\Omega_M = 0.3$, and $\Omega_\Lambda = 0.7$ for deriving the luminosities in Table 2. In converting from corrected broadband (X-ray 0.1–2.4 kev, and optical g-band) fluxes to luminosities, we again assume an X-ray power-law spectrum with energy index $\alpha_x = 1.5$, and an optical power-law with energy index $\alpha_o = 0.5$. The *9th column* lists α_{ox}, the slope of a hypothetical power law in energy from the UV/optical to X-ray (i.e., connecting 2500 Å and 2 kev). The *10th column* provides brief comments, for example noting selected objects that are radio sources, listing an alternate name (shortened, if needed, to the first 20 characters) taken from NED for about 10% of the quasars, and noting the ∼1.5% of the cases where two of our cataloged AGN fall within the same RASS error circle. (The latter are denoted by 'ambigID' in the comments, and eight such cases involve AGN pairs at similar redshifts). Again, only the initial five entries are included in the sample Table 2 within this paper itself; the full table is available electronically from the journal.

3.2. X-ray Emitting AGN Having Narrower Permitted Emission Lines

We have also examined the remainder of the 15,129 spectra of SDSS objects in RASS error circles, as some bona fide AGN identifications will fail to satisfy the broad-line (based on a simple single-component Gaussian pipeline fit) criterion discussed in the previous section. Our experience from Paper 1 verified that examining all relevant spectra helps insure fuller inclusion of such X-ray emitting AGN subclasses as NLS1s (see §4.1 for NLS1 details), Sy 1.5s, 1.8s, and 1.9s, i.e., objects with broad-line regions related to those of classic quasars and Seyfert 1s, but which may be observed to have "narrower" (< 1000 km s^{-1}) permitted-line components as well. The catalog of "narrow-line" AGN presented in this section is also extended to include Seyfert 2 and type 2 quasar candidates, whose optical spectra are even more strongly dominated by narrow emission lines. The additional narrow line AGN cataloged in this section are mainly from the lower redshift regime of our sample.

Following Paper 1, for classification among this narrower-lined group as Sy 1.5 to Sy 1.8, we manually verify from each SDSS spectrum that the full width near the continuum level (hereafter, FWZI) of the Hβ emission line exceeds 2500 km s^{-1}, also verifying that the width of the Hβ line exceeds that of the [OIII] 5007 emission in the same object by at least ∼1000 km s^{-1}. Hence each such object has some "broad-line" component substantially wider than typical of its narrow line region.

We also select among the narrow-line group, AGN whose SDSS optical spectra lack strong broad Hβ emission, but which nonetheless do have a markedly broad (at least at the continuum level) Hα emission component. As in Paper 1, we again refer to these objects loosely as Sy 1.9s, though many may be Sy 1.5-1.8, where S/N is merely low near Hβ. As in Paper 1, we again very conservatively limit our Sy 1.9 candidate list to include just those cases with very broad Hα, requiring FWZI(Hα)>6000 km s^{-1}. (Note that many Sy 1.9s were properly identified by the DR5 pipeline as broad-lined AGN based on the FWHM of Hα, and so are already cataloged in the current paper under the broad-line criteria in §3.1).

Our narrow-line catalog also includes candidate X-ray emitting Sy 2s and related AGN. We reemphasize the warning of Paper 1 that historically a number of such possible cases found in earlier X-ray surveys

have, when subsequently scrutinized with improved optical spectroscopy, ultimately been reclassified (e.g., Halpern, Turner, & George 1999) into one of the categories already considered above, e.g., NLS1, Sy 1.8, or Sy 1.9. Inclusion of these X-ray emitting Sy 2 candidates may, at the very least however, call attention to especially subtle cases of X-ray emitting Sy 1.8-1.9s or NLS1s that we otherwise might have missed. For most Sy 2 candidates, we again adopt the criteria of Kewley et al. (2001) based on the relative line strengths of [OIII]$\lambda 5007/H\beta$, [NII]$\lambda 6583/H\alpha$, and [SII]$\lambda 6717, 6731/H\alpha$; these line ratios define regions in "BPT diagrams" (Baldwin et al. 1981) populated by AGN versus starbursts. For a few objects, especially those at $z > 0.5$ where $H\alpha$, [NII], and/or [SII] measures are not available, we require only that [OIII]$\lambda 5007/H\beta > 3$. Note that we use the SDSS pipeline Gaussian line flux measures in this application. Tables 3 and 4 respectively catalog empirical and derived information for the additional 515 X-ray emitting narrower lined AGN discussed in this section; 405 of these have some observed broad-line component (e.g., NLS1s and Sy 1.5-1.9s), and an additional 110 are Sy 2 or type 2 quasar candidates. The comment column in Table 4 may include the spectral subclass type; these taxonomical classifications are tabulated to clarify why these narrower line AGN did not satisfy the broad-line criteria discussed in section 3.1 Again, only sample tables are included within this paper, with the full tables available electronically. Figure 3 shows selected SDSS spectra from this group of identifications, reflecting some of the diversity among these narrower lined X-ray emitting AGN.

3.3. BL Lac Candidates

We have also expanded our RASS/SDSS sample of BL Lac candidates to SDSS DR5. In Paper 1 we provided a list of 45 X-ray emitting BL Lacs and candidates, and additional cases from SDSS were presented as a subset of the more general spectroscopically-selected SDSS optical BL Lac sample discussed in Collinge et al. (2005). The rarity of BL Lacs demands large areal sky coverage such as that achievable from SDSS, and their unusual spectral energy distributions (with a lack of strong spectral features) generally allows efficient selection only via multi-wavelength approaches—especially in radio, optical, and X-ray surveys (e.g., Stocke et al. 1991, Perlman et al. 1996, Laurent-Muehleisen et al. 1997, Bade et al. 1998a; also see review by Urry & Padovani 1995).

We employ similar approaches within our 'ROSAT_A' target selection algorithm (as discussed in section 2), to obtain the updated DR5 sample of RASS/SDSS BL Lac candidates discussed here. We find (or recover) 181 objects we consider as *probable* X-ray emitting RASS/SDSS BL Lacs. For these higher confidence cases: (1) the SDSS optical object is within $1'$ of a RASS source; (2) the SDSS object is also a positional match to a radio source (conservatively taken as $< 2''$ for matches to FIRST sources, or $< 7''$ for matches to other radio catalogs); (3) our measures from the SDSS optical spectrum reveal no strong emission ($EW < 5$ Å); and, (4) either there is no CaII H&K break/depression evident in the SDSS optical spectrum, or if present any such break must be weak. Following Stocke et al. (1991), we require the CaII H&K break to have $C \leq 0.25$, where $C = 0.14 + 0.86(f_{\lambda,+} - f_{\lambda,-})/f_{\lambda,+}$ and where $f_{\lambda,-}$ and $f_{\lambda,+}$ are the average specific fluxes over the wavelength ranges 3750-3950 and 4050-4250 Å, respectively (e.g., see Landt et al. 2002, Dressler & Schectman 1987). We also find as *possible* BL Lac candidates 85 additional objects that are within RASS error circles and which either: satisfy the first three criteria (X-ray/radio sources with no strong optical emission), but which have slightly larger CaII H&K breaks with $0.25 < C < 0.4$ (see Marchã et al. 1996); or, have too low S/N in their SDSS optical spectra to claim with confidence the BL Lac spectral nature of criteria (3) and (4); or, which show approximately featureless SDSS spectra, i.e., that satisfy criteria (1), (3), and (4), but where there is no close match to a radio source. The latter seven objects

are of potentially high interest for additional follow-up as unusually weak radio sources; the vast majority of confidently-identified BL Lacs cataloged thus far are radio sources (though some are weak).

The 5740 deg^2 of sky considered here thereby include a total of 266 candidate X-ray BL Lac counterparts, and basic information for them is provided in Tables 5 and 6. Again, only the initial 5 entries are included in these sample tables; the full tables are available electronically from the journal. An entry of 'zunc' in the comment column of Table 6 denotes cases where a redshift from SDSS or the literature is unavailable or highly uncertain. If a redshift is not obtained from the SDSS spectrum, nor available in the literature, we adopt $z = 0.3$ (near the median of others in the sample) for estimating α_{ox} in Table 6; as this is essentially a distance-independent ratio of luminosities, the values of α_{ox} should be approximately correct in most cases, except for precise values of spectral K-corrections. In Table 6, we denote the possible but less certain BL Lac candidates as 'BL?' in the comment column. Example SDSS spectra of representative X-ray BL Lac candidates are shown in Figure 4.

About half of these objects were first identified as BL Lac candidates via SDSS, and/or have redshifts first reliably measured from SDSS spectroscopy. (Though some, for example, are cataloged in Bade et al. 1998b, but lacked secure identifications and/or redshifts in their low-resolution prism data). About 40% of the full sample of 266 currently have reasonably confident SDSS or published spectroscopic redshifts, and another 20% less confident spectroscopic redshift estimates.

As an added precaution to limit contamination of the BL Lac sample by stars with weak features (e.g., DC white dwarfs), we have also considered proper motion information, as in Collinge et al. (2005). We obtained proper motions from the SDSS database for 242 of our 266 RASS/SDSS BL Lac candidates. Of these 242, only four BL Lac candidates appear to have significant proper motion (>20 mas/yr). However, three of the latter candidates have secure extragalactic redshifts from their SDSS spectra, and the fourth object is cataloged as a confirmed BL Lac in Veron-Cetty & Veron (2006). All four candidates additionally match to both an X-ray and a radio source, suggesting little contamination by nearby hot white dwarfs. Thus, it seems likely that most of the BL Lac identifications are correct (see also section 5 below).

This catalog of RASS/SDSS/radio selected BL Lac candidates constitutes one of the largest samples obtained to date (see also Collinge et al. 2005, for a similarly large optically-selected sample from SDSS). Each is accompanied by uniform X-ray, optical, and radio data.

4. Other Rare Classes of X-ray Emitting AGN

4.1. Narrow-line Seyfert 1s (NLS1s)

In our expanded DR5 RASS/SDSS sample we identify from SDSS spectra a total of 774 candidate X-ray emitting NLS1s. These include objects cataloged in both sections 3.1 and 3.2, and they are denoted by 'NLS1?' in the comment columns of Tables 2 and 4. Williams et al. (2002) discussed 45 of these SDSS X-ray NLS1s independently selected from the SDSS Early Data Release, and we added 120 more in Paper 1. In the optical, NLS1s have unusually narrow permitted lines, though in most other ways resemble Sy 1s more than Sy 2s; in the X-ray, they often show strong soft X-ray excesses and marked variability. Various explanations have been suggested for NLS1s, e.g., unusually low-mass black holes and/or higher accretion rates relative to Eddington, etc. (see reviews by Boller 2000 and Pogge 2000).

The 774 X-ray emitting candidate NLS1s all have the following spectral characteristics, representative of the NLS1 class (e.g., Pogge 2000): [OIII] λ5007 to $H\beta$ flux ratios of less than 1 (from the SDSS spectroscopic

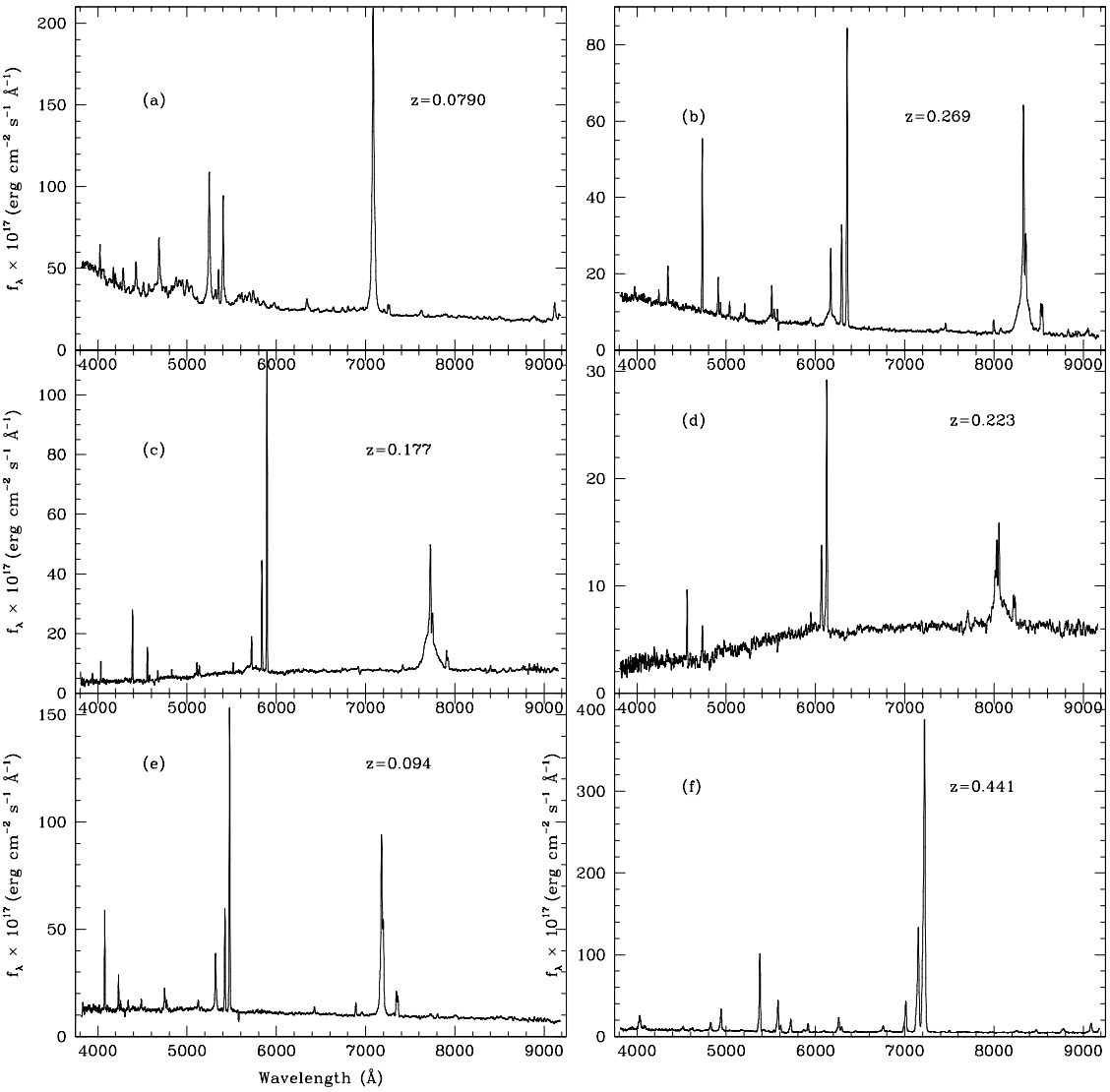

Fig. 3.— Selected SDSS optical spectra for RASS/SDSS X-ray emitting quasars/AGN with narrower permitted emission components, chosen to reflect the diversity among the 515 objects cataloged in section 3.2. Approximate spectral taxonomical classifications for (a-f) are, respectively: NLS1, Sy 1.5, Sy 1.8, Sy 1.9, Sy 2, and a possible type 2 quasar (see Zakamska et al. 2003 for a discussion of SDSS type 2 quasars). (a) SDSS J141755.54+431155.8; (b) SDSS J142337.63+341052.9; (c) SDSS J155021.40+295027.8; (d) SDSS J085348.18+065447.1; (e) SDSS J143001.63+455049.1; (f) SDSS J091345.48+405628.2.

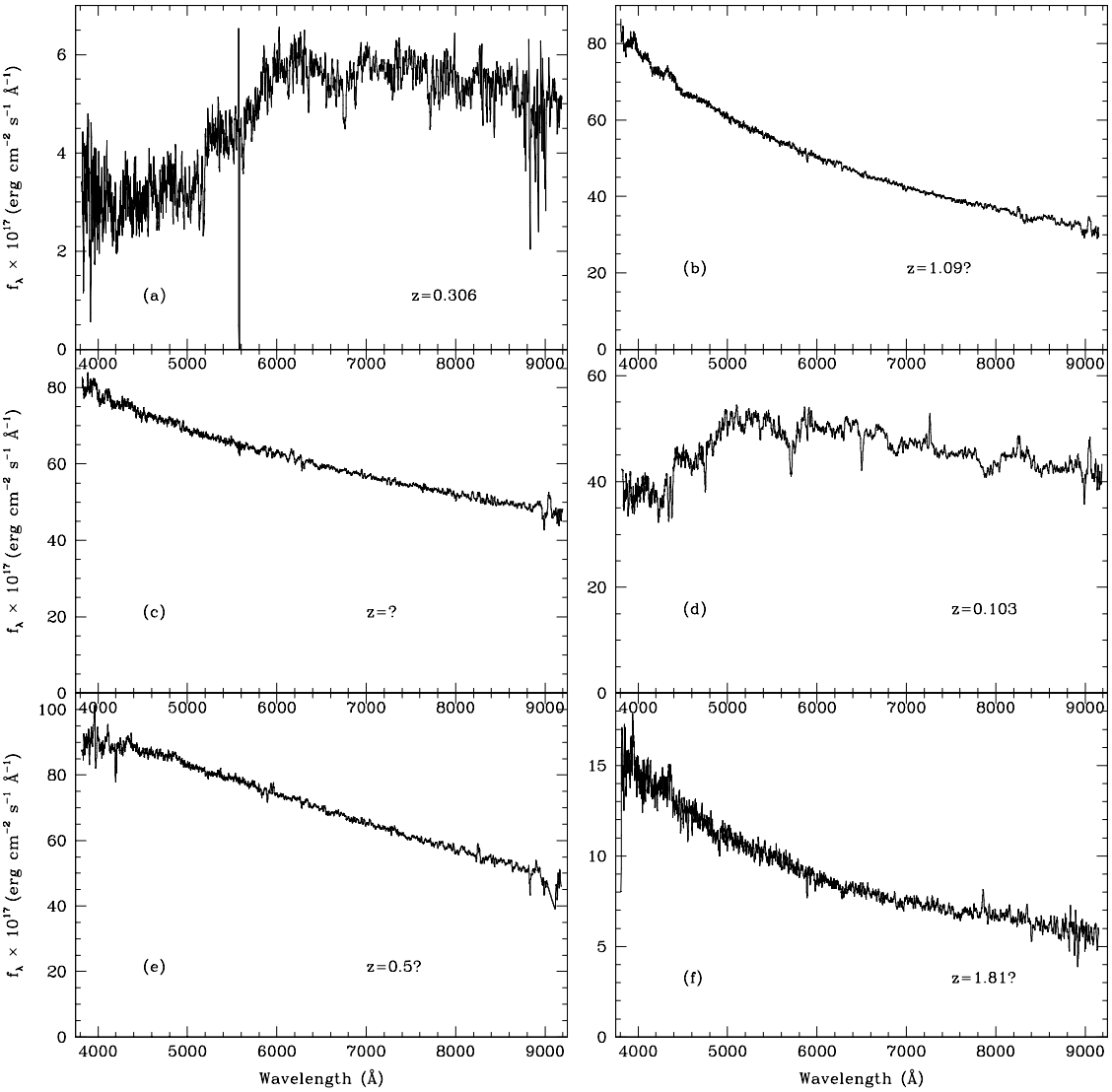

Fig. 4.— Representative SDSS optical spectra for RASS/SDSS X-ray emitting BL Lac candidates as discussed in section 3.3. Shown (a-e) are spectra for the first 5 objects listed in Tables 5-6, along with a possible high-redshift case (f). A total of 266 such BL Lac candidates are presented in our updated RASS/SDSS catalog. (a) SDSS J002200.95+000657.9; (b) SDSS J003514.72+151504.1; (c) SDSS J005041.31−092905.1; (d) SDSS J005620.07−093629.8; (e) SDSS J014125.83−092843.6; (f) SDSS J124700.72+442318.7.

pipeline Gaussian-fit emission line measures), Hβ FWHM (again from the SDSS spectroscopic pipeline) less than 2000 km s^{-1}, and strong optical Fe emission. Seventy-four of these are detected in the FIRST radio survey; these are of possible special interest, as radio-loud NLS1s may be unusually rare (e.g., Komossa et al. 2006). An example SDSS spectrum for a NLS1 candidate is shown in Figure 3a.

4.2. BALQSOs

ROSAT studies extending back more than a decade (Green et al. 1995), along with many subsequent investigations, demonstrated that BALQSOs as a class are weak emitters in soft X-rays. The soft X-ray deficiency is thought to arise due to absorption in BAL material of high column density, typically inferred equivalent to $N_H \sim 10^{22-23}$ cm^{-2} (e.g., Green et al. 2001; Gallagher et al. 2002). In our DR5 sample, there are 14 cases of traditional BALQSOs (e.g., those with "balnicity-index" $BI > 0$) that fall within $1'$ RASS error circles, plus another two dozen cases with weaker BALs and/or possible mini-BALs. (See Trump et al. 2006 for an extensive recent discussion and catalog of SDSS BALQSOs, selected based on both the standard Weymann et al. 1991 BI criteria, as well as the more inclusive "absorption line" index or AI criteria of Hall et al. 2002). Of course, in some cases an improved X-ray position may be required to definitively establish whether or not all these BALQSOs are actually the X-ray source counterparts, given the expected (see §5) few percent contamination of our full AGN sample. Shown in Figure 5a is the SDSS spectrum of an example X-ray emitting BALQSO.

Although definitive conclusions await further confirmations of which BALQSOs are genuine X-ray sources and which are just chance coincidences, the RASS/SDSS sample size is now large enough to begin to provide some ensemble statistical tests of the (anticipated low) incidence of X-ray emitting BALQSOs. For example, the Trump et al. (2006) SDSS study found an incidence of 10.4% (with a formal statistical error of about 0.2%) for mainly optically-selected $BI > 0$ BALQSOs among DR3 quasars with $z > 1.7$. The analogous BALQSO incidence in our RASS/SDSS X-ray selected sample is $4.6\% \pm 1.5\%$, i.e., a significantly smaller incidence in a soft X-ray selected sample (at least) at the $> 3\sigma$ level. In the latter estimate we consider just the DR3 subset for maximum consistency with the Trump et al. study; this is really an upper limit on the incidence in the RASS/SDSS sample, as it somewhat optimistically assumes that all $BI > 0$ cases are genuine X-ray/BALQSO associations.

4.3. Unusual Line-Profile and Other Odd Cases

There are many further quasars in our updated catalog with unusual optical line profiles (see Paper 1 for further discussion). These include further examples of X-ray emitting AGN with weak/narrow Hβ characteristic of Sy 1.8-2s but also having strong broad MgII (Figure 5b), post-starburst AGN (Figure 5c), AGN with broad asymmetric Balmer profiles (Figures 5d-e), and X-ray AGN with highly unusual multiple-peaked emission line profiles (Figures 5e-f).

5. Ensemble Properties and Identification Reliability

From the expanded 5740 deg^2 of sky coverage in DR5, 7000 quasars or other AGN are identified as likely RASS counterparts, each with uniform and high-quality optical photometry and spectroscopy from

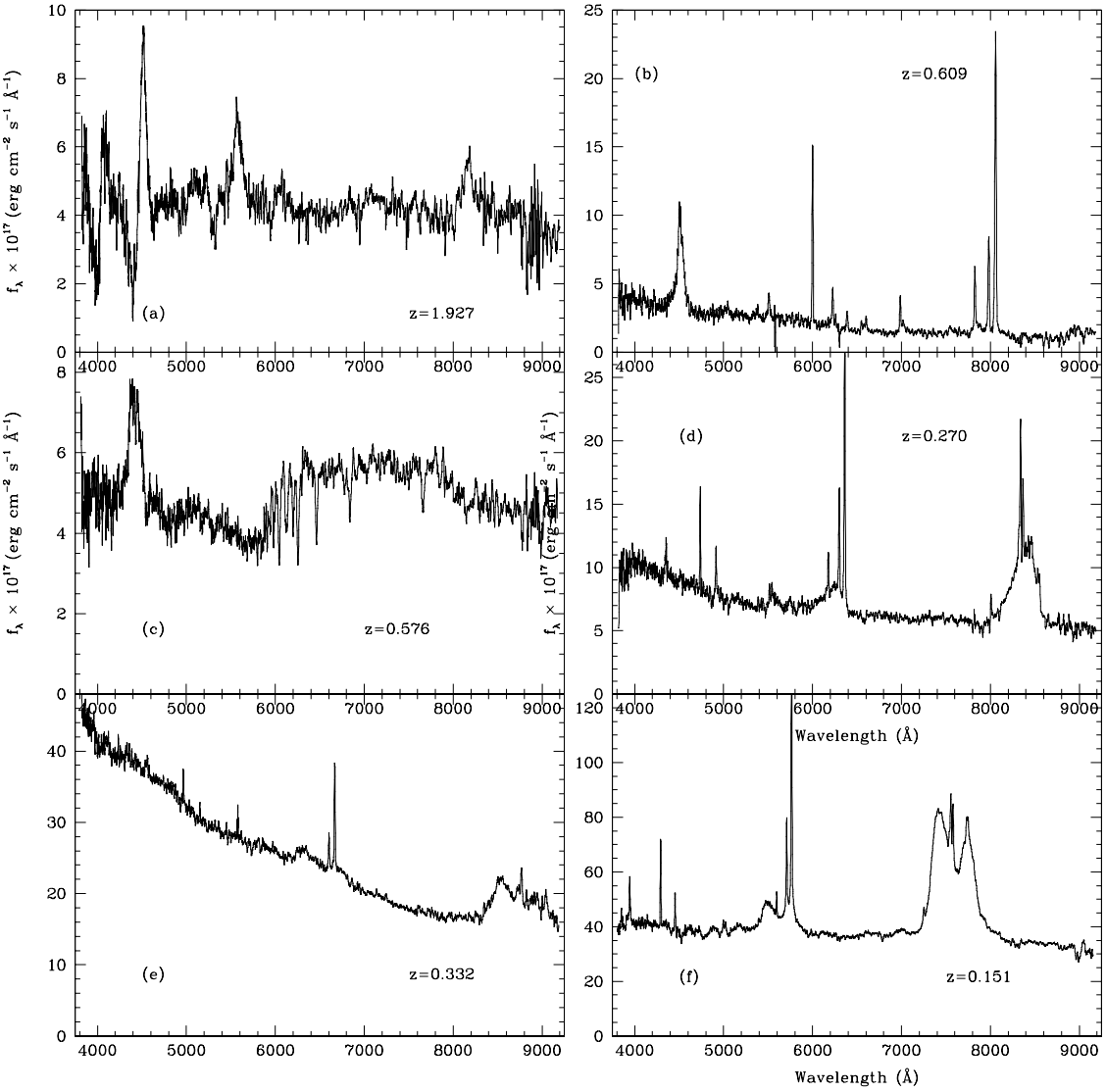

Fig. 5.— Selected other RASS/SDSS X-ray emitting AGN having unusual optical SDSS spectral characters. (a) SDSS J105626.95+482956.3 is example of a possible X-ray emitting BALQSO. (b) SDSS J074951.42+204936.9 is an AGN with weak/narrow Hβ characteristic of Sy 1.8-2, but which has strong, broad MgII. (c) SDSS J163446.49+461946.7 is a post-starburst AGN. SDSS J115227.12+604817.4 (d) and SDSS J102738.53+605016.5 (e) are examples of AGN with broad, asymmetric Balmer profiles. (f) SDSS J161742.53+322234.3 is an example X-ray emitting AGN with unusual multiple-peaked and broad emission lines profiles (SDSS J1027+6050 may also be double-peaked).

SDSS, and X-ray data from ROSAT. The ensemble X-ray flux, optical magnitude, and redshift distributions are depicted in Figure 6. The X-ray flux distribution (Figure 6a) reflects the typical depth of the RASS catalogs, with median $f_x = 2.5 \times 10^{-13}$ erg s^{-1} cm^{-2}; the optical magnitude (Figure 6b) and redshift (Figure 6c) distributions of the AGN remain typical of past identification work at comparable X-ray depth, with medians $g = 18.8$ and $z = 0.42$. However, our updated RASS/SDSS catalog is sufficiently large to, for example, include 162 $z > 2$ X-ray emitting AGN, 334 having $g < 17$, and 505 with $f_x > 10^{-12}$ erg s^{-1} cm^{-2} Note that in our sample, which is affected by both X-ray and optical flux limits, luminosities and redshift are strongly coupled (Figure 7).

In our expanded DR5 catalog, the distributions of offsets between RASS X-ray positions and SDSS optical positions are again approximately as expected, if most of the 7000 AGN are the proper identifications. For example, 86% of the SDSS quasars/AGN fall within 30″ of the RASS X-ray positions (see the angular offset distribution in Figure 8a), in approximate agreement with the RASS positional uncertainty distribution, independently derivable from Tycho stars also detected in RASS (Voges et al. 1999). In Figure 8b, these angular offsets have been normalized relative to their associated estimated RASS positional errors, to better account for the dependence of the RASS positional uncertainty on the X-ray source significance, etc. This figure confirms that the RASS positional error estimates are reasonable, with 98% of the suggested identifications at offsets smaller than 3σ (where σ is the estimated RASS X-ray positional error); we also note, however, that the distribution of RASS positional errors may not be fully characterized by either a simple 1- or 2-dimensional Gaussian (Agüeros et al. 2006). Figure 9 shows the distributions of the squares, r^2, of the offsets between the SDSS optical positions and the RASS X-ray source positions for various AGN subclasses considered herein; specifically, we display the fraction of suggested SDSS counterparts falling within equal area annuli offset from the RASS X-ray source positions. For a chance superposition of SDSS objects within RASS error circles, these histograms would be approximately flat with r^2. But the respective distributions for broad-line AGN (from §3.1), narrow line AGN (§3.2), BL Lacs (§3.3), and NLS1s (§4.1) are each strongly-peaked at small r^2 values, as expected if these AGN are statistically the proper X-ray source identifications.

Further quantifying the statistical reliability of these identifications is the following. The surface density of SDSS optically-selected quasars is a little more than 12 deg^{-2} (e.g., Schneider et al. 2005), while the combined area covered by all RASS error circles considered in the 5740 deg^2 area of this updated sample is a little over 13 deg^2. Thus, based on surface density arguments, only a small fraction (of order 3%) of the proposed quasar/AGN X-ray source counterparts are likely to be spurious random chance positional coincidences. Similarly, if we randomly alter the positions in the RASS catalog by several arcminutes, and then cross-correlate again between SDSS quasars and such synthetically-offset RASS catalogs, we alternately estimate that only of order 5% of the SDSS AGN cataloged herein are likely to be chance positional coincidences, unrelated to RASS X-ray sources.

The ratios, f_x/f_{opt}, of X-ray to optical flux for the identifications are also as expected for typical X-ray emitting AGN. Roughly as much energy is emitted in the X-ray as in the optical bands for typical quasars, as is reaffirmed by the empirical f_x/f_{opt} distribution shown in Figure 10a for the 6224 quasars/AGN with predominant broad emission line regions considered in section 3.1 In estimating f_x/f_{opt}, we here adopt the (corrected) 0.1-2.4 keV X-ray flux (e.g., from Table 2), and estimate the optical broadband flux in a 4000-9000 Å bandpass using the g-band PSF magnitudes (e.g., again from Table 2) assuming an optical power law in energy with index $\alpha_o = 0.5$. The observed f_x/f_{opt} distribution in Figure 10a for DR5 broad-line RASS/SDSS AGN appears very similar to that found for EMSS quasars (see Stocke et al. 1991); two-sided Kolmogorov-Smirnov (K-S) comparisons between the EMSS and RASS/SDSS f_x/f_{opt} distributions for

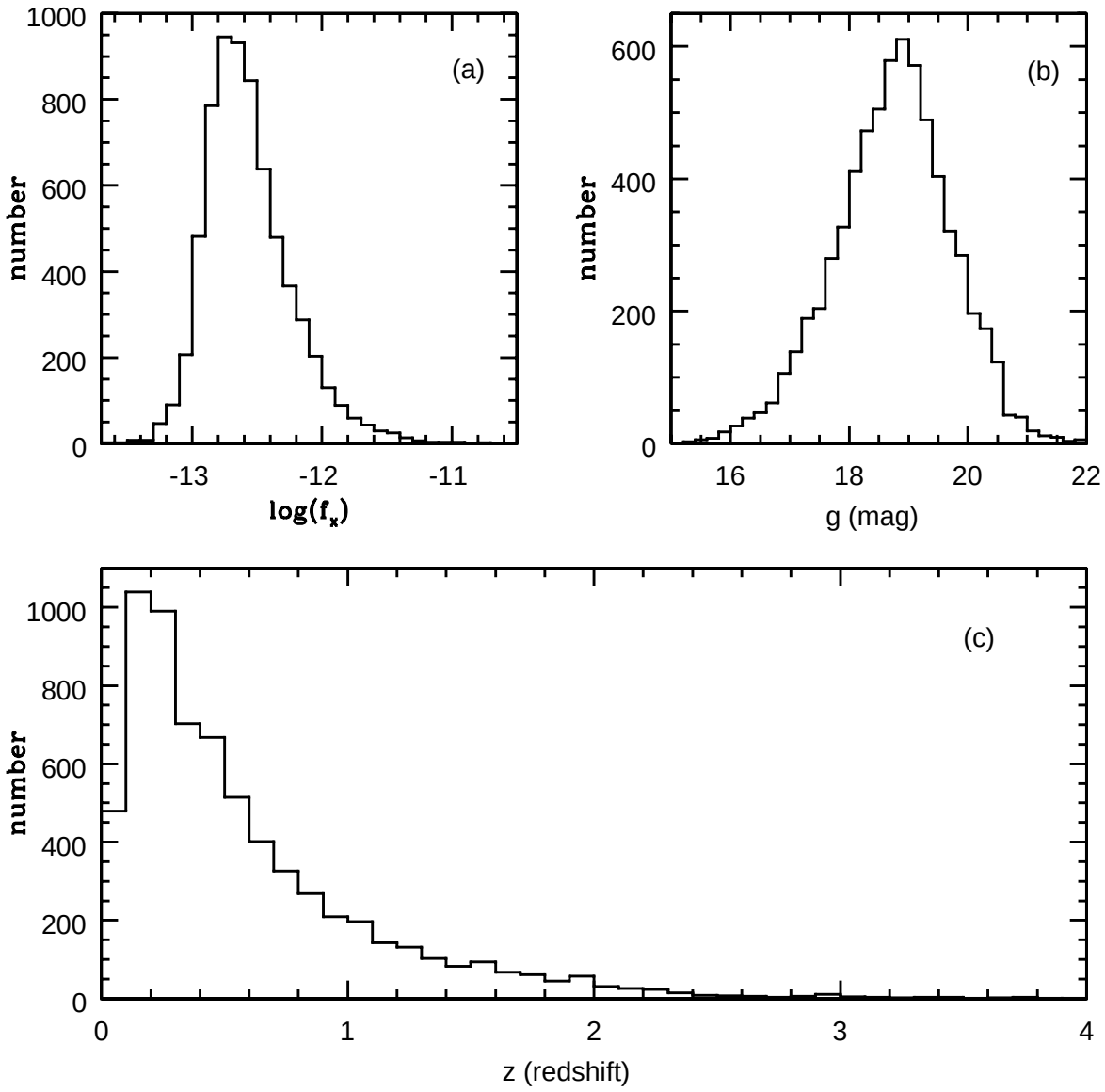

Fig. 6.— Distributions of (a) RASS X-ray fluxes, (b) SDSS g-band magnitudes, and (c) redshifts for 6700 AGN counterparts of RASS/SDSS X-ray emitting AGN. (BL Lacs are excluded from the plots here, as many have uncertain redshifts). The median magnitude ($g = 18.8$) and redshift ($z = 0.42$) are typical of other optical identification efforts at comparable X-ray depth (median $f_x = 2.5 \times 10^{-13}$ erg s^{-1} cm^{-2}), though the very large sample includes a substantial number of bright or higher redshift AGN as well.

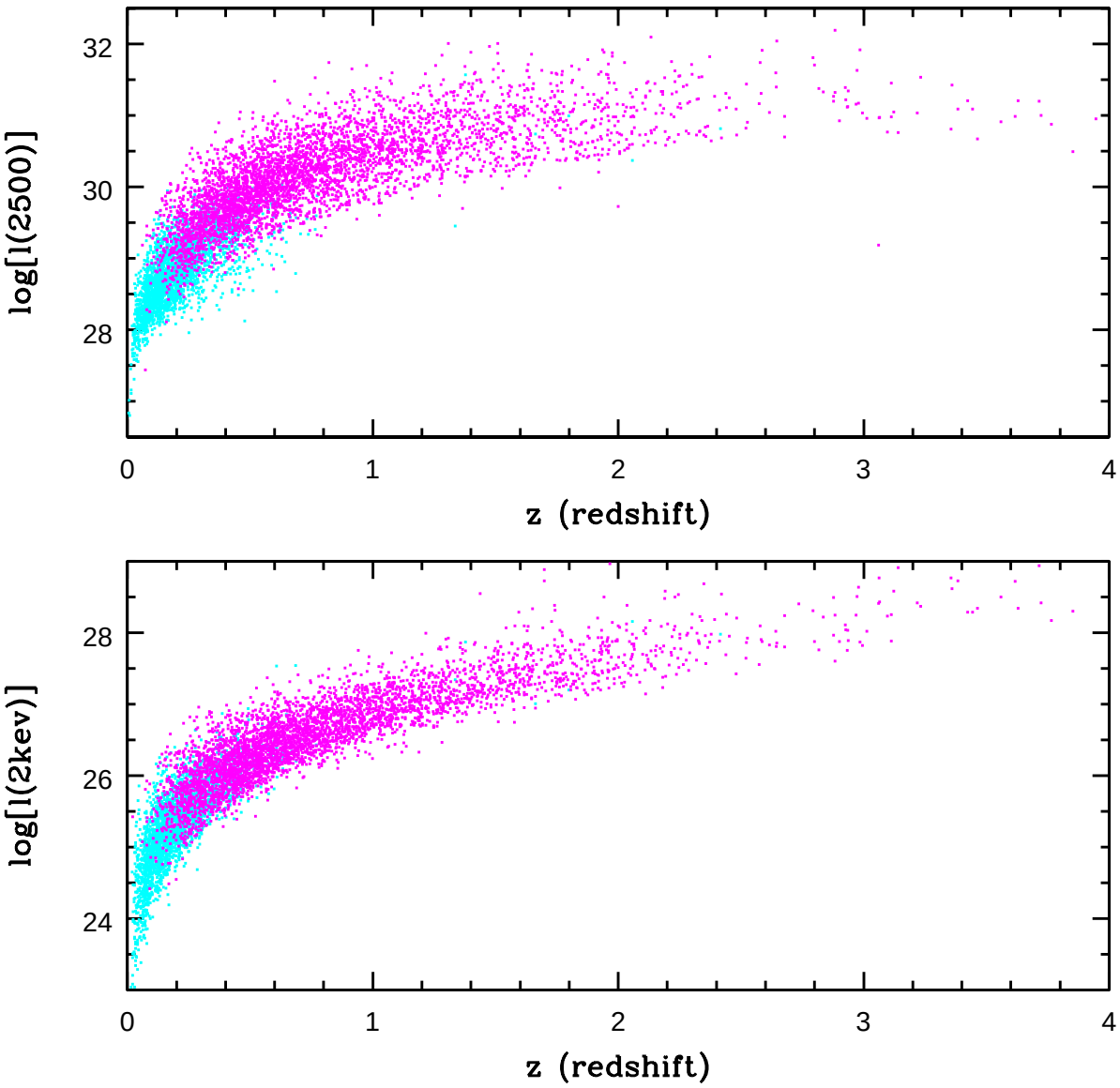

Fig. 7.— Luminosities and redshift are strongly coupled in our sample with both X-ray and optical limits (cgs monochromatic luminosities at frequencies corresponding to 2500 Å and 2 keV are shown). The *magenta* points display data for quasi-stellar X-ray identifications that are unresolved in SDSS optical images, while *cyan* points show data for AGN that are morphologically resolved in SDSS.

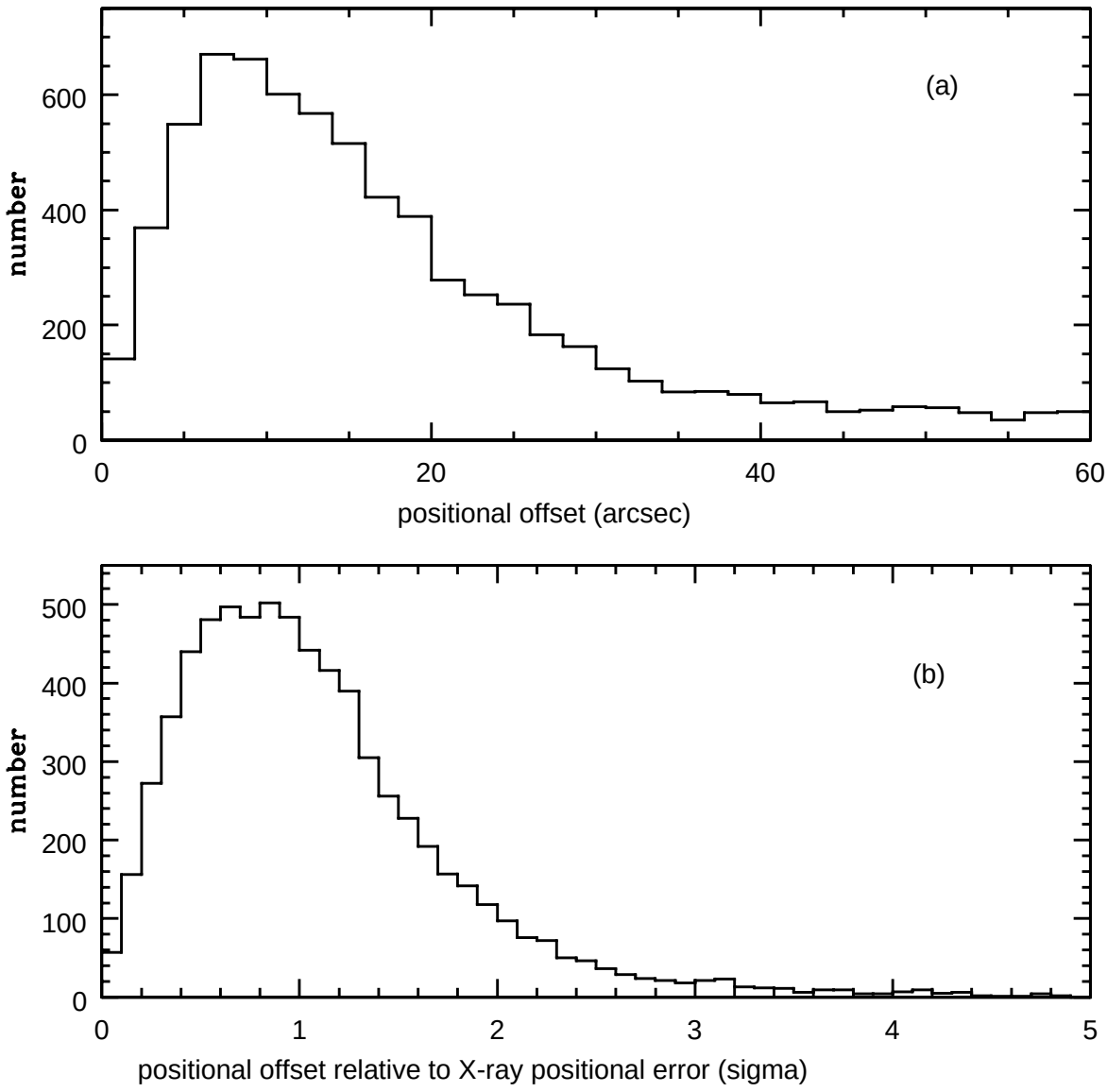

Fig. 8.— The distribution of differences between the SDSS optical and RASS X-ray positions of the 7000 AGN cataloged here are consistent with expectations, if most are the proper identifications. (a) The positional offset distribution in arcseconds is approximately as expected for the RASS positional accuracy. (b) The distribution of the differences between the SDSS optical and RASS X-ray positions, here normalized by their associated RASS X-ray source positional errors. (A handful of objects with relative offsets $> 5\sigma$ are excluded from this plot).

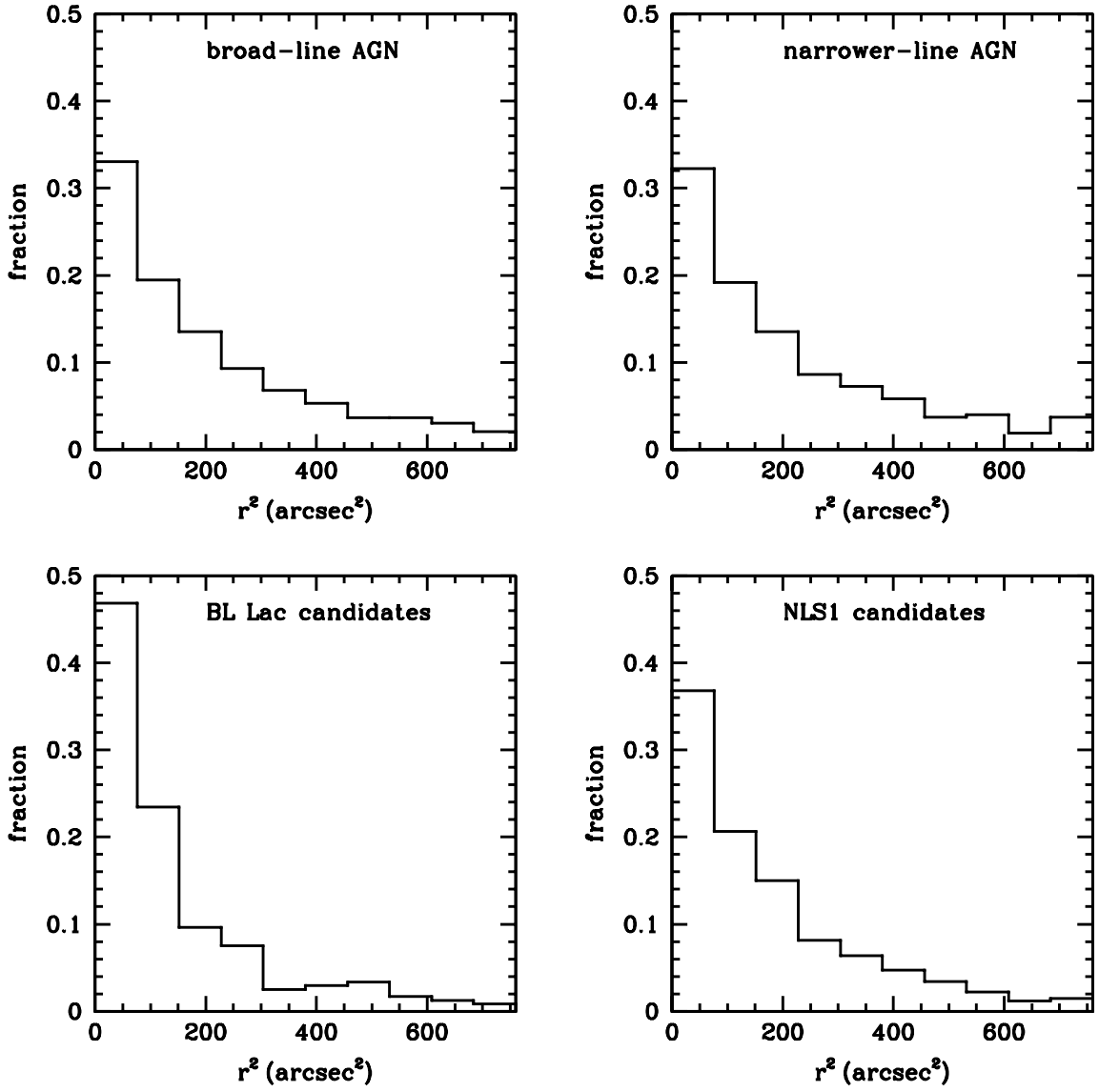

Fig. 9.— Distributions of the squares, r^2, of the offsets between the SDSS optical positions and the RASS X-ray source positions; specifically, we display the fraction of optical counterparts falling within equal area annuli offset from the RASS X-ray source positions. (We consider only objects within $r < 27.5''$, where all relevant algorithms for SDSS spectroscopy may select targets). Distributions are shown for quasars/AGN with predominant broad-lines discussed in section 3.1 (upper left), quasars/AGN with narrower permitted lines discussed in section 3.2 (upper right), BL Lac candidates discussed in section 3.3 (lower left), and candidate NLS1s discussed in section 4.1 (lower right). In each case, the distributions are very strongly-peaked at small r^2 values, as expected if these AGN are statistically the proper X-ray source identifications.

quasars confirm similarity at the 23 to 61% level, for a plausible range of conversions between the differing EMSS versus RASS/SDSS X-ray and optical passbands (and implicit spectral assumptions). Figure 10b shows the analogous distribution of f_x/f_{opt} ratios for the 266 RASS/SDSS BL Lac candidates discussed in section 3.3. This distribution also appears very similar to that found in earlier X-ray selected BL Lac samples (e.g., again see Stocke et al. 1991); two-sided K-S tests indicate a match of EMSS and RASS/SDSS f_x/f_{opt} distributions for BL Lacs at the 21 to 64% level, with the range again reflecting uncertainties in conversions between systematically different passbands, etc. The broad agreement of the f_x/f_{opt} distributions with previous work for both quasars and BL Lacs further confirms that the vast majority of the suggested RASS/SDSS identifications are likely correct.

6. An Example X-ray/Optical Correlation from the Expanded Sample

This paper primarily presents updated catalog information, but we also include below a brief update on our Paper 1 example of an X-ray/optical correlation. More generally, the large RASS/SDSS sample size and associated uniformity of X-ray and optical (and radio) data may be useful for other more detailed, multiwaveband follow-on studies (e.g., see Körding et al. 2006).

The 6224 X-ray emitting AGN with predominant broad-line regions discussed in section 3.1 show (see Figure 11) the well-known correlation between (the logarithms of) optical and X-ray monochromatic luminosities found in many earlier studies/samples (e.g., Avni & Tananbaum 1986). We again caution (see Paper 1) that our sample is, of course, an X-ray selected sample with inherent X-ray biases. Nonetheless, the best-fit linear relationship we find (Figure 11a) between the logarithms of X-ray and optical luminosities, equivalent to $l_x \propto l_{opt}^{0.90\pm0.01}$, is in good agreement with that found in other studies (e.g., see Wilkes et al. 1994; Green et al. 1996; Vignali et al. 2003; Paper 1). This best-fit linear relation is virtually unchanged when excluding the 15% of the objects that are radio-detected.

As we suggested previously in Paper 1, however, the best-fit slopes of the relation within our RASS/SDSS sample differ when separately considering lower versus higher optical-luminosity objects. For example, if we divide the 6224 broad line AGN (§3.1) into two subsamples at the median value $log(l_{opt}) = 29.76$ (cgs), we find $l_x \propto l_{opt}^{0.96\pm0.01}$ for the half below the median, but $l_x \propto l_{opt}^{0.85\pm0.02}$ for the half above the median optical luminosity; both these slope values are consistent with those we quoted in Paper 1—though from a much smaller sample in that earlier paper—for a very similar luminosity division. If one restricts consideration to just the 406 objects in our DR5 sample with highest optical luminosity $log(l_{opt}) > 31$, the best-fit slope of the logarithmic relation decreases even further, corresponding to $l_x \propto l_{opt}^{0.50\pm0.09}$. Very recently, some large studies (Steffen et al. 2006) based on optically-selected samples have also begun to confirm that the best-fit slope in the relationship between $log(l_x)$ and $log(l_{opt})$ may not be a constant, but instead may itself depend on optical luminosity. Such a "non-linear" relationship between $log(l_x)$ and $log(l_{opt})$ was suggested in our Paper 1 and earlier studies such as those of Yuan et al. (1998a). Such complicated possible dependences caution that when considering results among different studies, it is useful to compare X-ray versus optical correlations for objects of similar luminosity.

One might alternately divide the sample between morphologically-resolved AGN and those that have optical stellar-PSF morphology in SDSS images (see the type parameter in Table 1). With this sub-division, one finds a similar result: $l_x \propto l_{opt}^{0.97\pm0.02}$ for resolved AGN compared with $l_x \propto l_{opt}^{0.84\pm0.01}$ for stellar-morphology AGN. Not too surprisingly, however, the resolved AGN (for which optical host galaxy photometric contributions may be most problematic) are at systematically lower optical luminosity and redshift than the

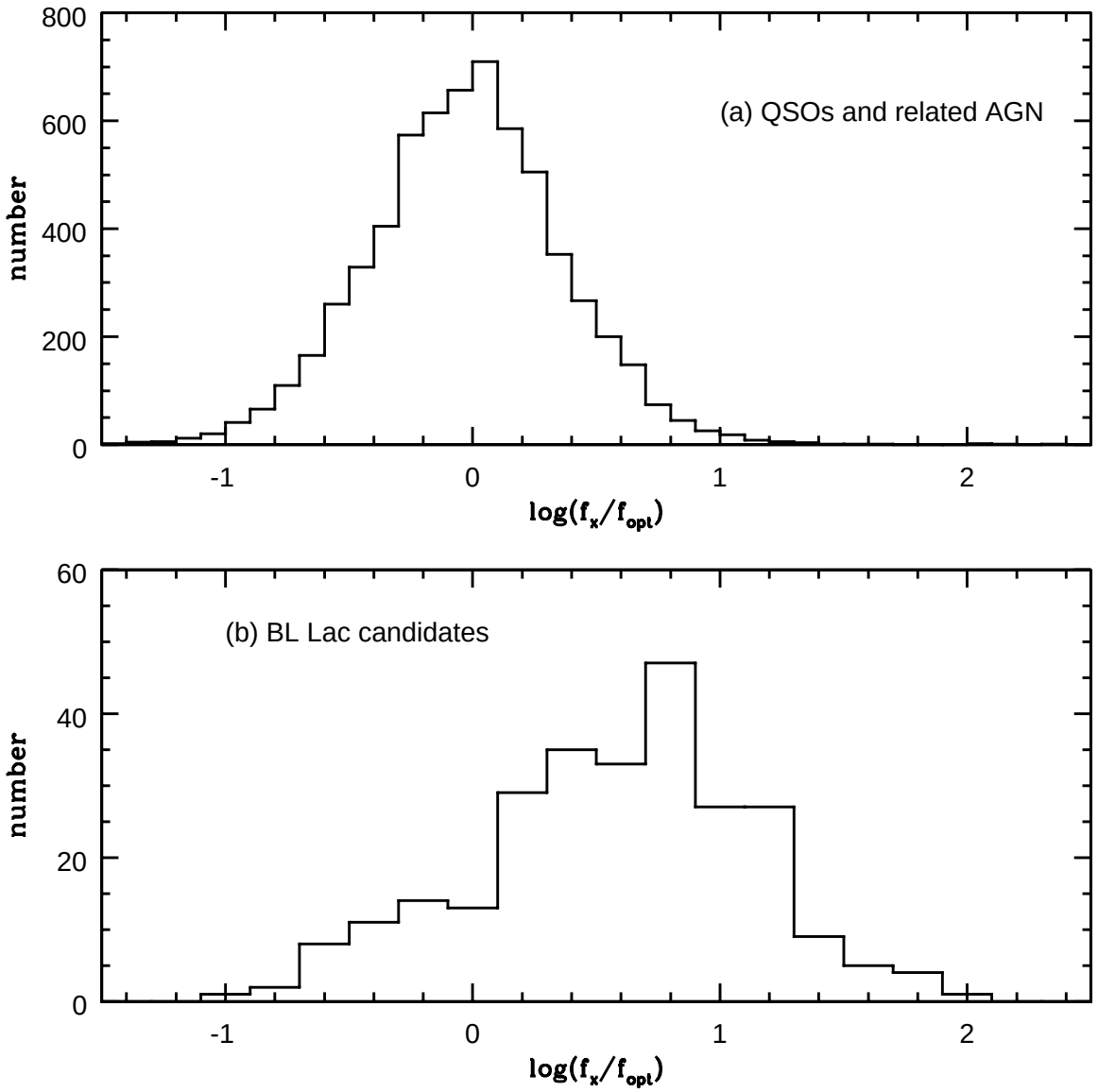

Fig. 10.— (a) The f_x/f_{opt} distribution for the 6224 quasar/AGN identifications having predominant broad emission line regions (see §3.1). The RASS/SDSS quasars/AGN emit approximately as much energy in the X-ray as in the optical band, as expected if these are the proper identifications. (b) The f_x/f_{opt} distribution for the RASS/SDSS BL Lac candidates discussed in section 3.3. The distribution is similar to that found in other X-ray selected BL Lac surveys, affirming that these RASS/SDSS objects are also likely to be the proper identifications.

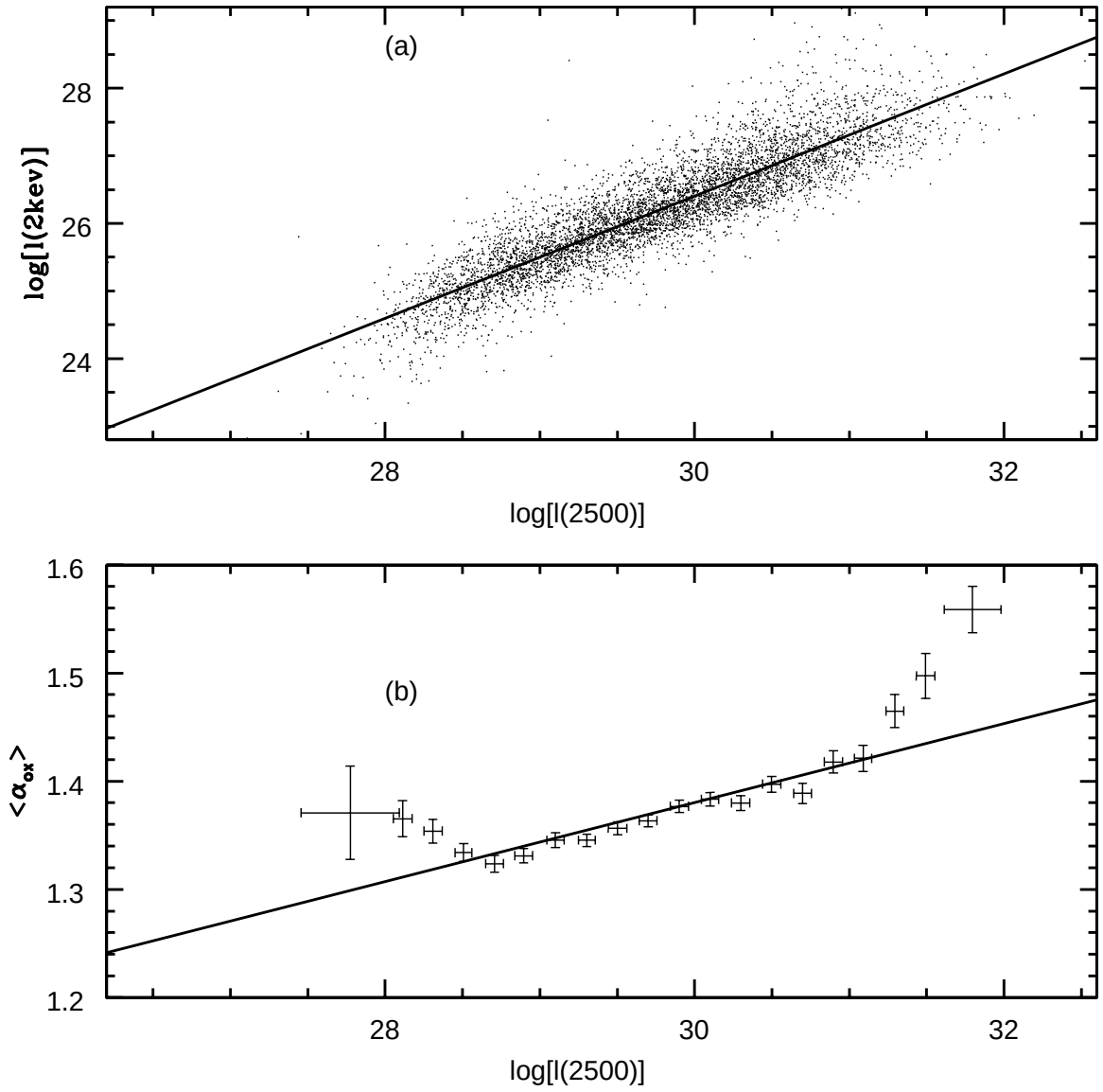

Fig. 11.— The well-known relationship between X-ray and optical wavebands (logarithms of monochromatic luminosities in cgs units at 2 kev and 2500Å are used) is also seen here in our X-ray selected sample of 6224 quasars/AGN with predominant broad emission line regions. (a) The solid line is a linear least-squares fit to the logarithms of l_{2kev} versus l_{2500} data, with slope 0.90 ± 0.01. (b) Consistent results are obtained when regressing α_{ox} against optical luminosity, and in this case a simple linear regression yields $\alpha_{ox} \propto l_{opt}^{0.037}$, equivalent as expected to $l_x \propto l_{opt}^{0.90}$. The solid line is the best-fit linear regression relation when fit to all 6224 points separately; the error bars show the mean and the standard error in the mean value of $\langle \alpha_{ox} \rangle$, as well as the mean and standard deviations in optical luminosity, when considering averages taken in various logarithmic optical luminosity bins (typically with 100 to 500 points per bin). The deviation of multiple adjacent, and independent, error bars significantly away from the simple best-fit line suggests the possibility of a more complicated relation than assumed in standard linear regression models.

optically-unresolved subset (Figure 7). Further studies will be required to disentangle such strongly coupled parameters.

Regressing α_{ox} against optical luminosity yields similar results. For the 6224 quasars/AGN with observed broad-line regions discussed in section 3.1, this regression yields $\alpha_{ox} \propto l_{opt}^{0.037\pm0.002}$, approximately equivalent as expected to $l_x \propto l_{opt}^{0.90}$. Figure 11b depicts the relationship from the α_{ox} perspective. The solid line shows the above linear best-fit regression relation with slope 0.037, while the error bars show the mean and the standard error in the mean value of α_{ox}, as well as the mean and standard deviations of the optical luminosity, when considering averages taken in various logarithmic optical luminosity bins. (The vertical error bars account for the large number of data points averaged to estimate $\langle\alpha_{ox}\rangle$ in each bin: typically 100-500, with a range of 42 to 534). The offset of multiple independent and adjacent error bars significantly away from the simple best-fit line in Figure 11b, further suggests the possibility of a more complicated relation than assumed in the standard linear regression of α_{ox} versus $\log(l_{opt})$, or in the equivalent $\log(l_x)$ versus $\log(l_{opt})$ relation discussed above.

However, we reiterate our caution of Paper 1 that the multiple strongly correlated parameters involved here require a much more careful analysis, including proper accounting and disentangling of the various selection biases, intertwined dependences on redshift and optical luminosity, disparate dispersions in optical compared with X-ray luminosities (e.g., Yuan, Siebert, & Brinkmann 1998b), host galaxy photometric contamination, radio dependences, and so on. To highlight such complications, we note that two recent studies on optically-selected SDSS quasars having ROSAT information available arrive at rather different conclusions about whether α_{ox} may also depend on redshift as well as optical luminosity (Shen et al. 2006; Steffen et al. 2006). As noted above, certainly these two parameters (and others) are strongly correlated in our RASS/SDSS sample, with flux limits in both the X-ray and the optical (Figure 7).

7. Summary

The SDSS optical and RASS X-ray surveys are well-matched to each other, allowing efficient large-scale identification of X-ray source optical counterparts. Application of our approach to SDSS DR5 data has provided homogeneous identification and RASS/SDSS flux and spectroscopic data for a large sample of X-ray emitting quasars and other kinds of AGN. The combination of SDSS multicolor selection and RASS data—and in some cases FIRST radio information—is highly efficient for the selection of X-ray emitting quasars/AGN. In our updated analysis encompassing 5740 deg^2 of sky, 7000 plausible X-ray emitting quasars/AGN have been optically identified, including hundreds of rare cases such as BL Lacs and NLS1s. The RASS/SDSS survey is rapidly approaching $\sim 10^4$ fully and homogeneously characterized optical counterpart identifications. The large sample will allow for a variety of more detailed studies of various AGN subclasses and individual objects of special interest, as well as for studies of ensemble correlations between optical and X-ray wavebands. In closing, we also note that many of the cataloged objects have X-ray fluxes accessible to at least the next generation of envisioned high-quality X-ray spectroscopy experiments, such as Constellation-X.

Acknowledgments: S.F. Anderson and R.M. Plotkin gratefully acknowledge support from NASA/ADP grant NNG05GC45G. We thank Jonathon Trump for useful discussions.

Funding for the SDSS and SDSS-II has been provided by the Alfred P. Sloan Foundation, the Participat-

ing Institutions, the National Science Foundation, the U.S. Department of Energy, the National Aeronautics and Space Administration, the Japanese Monbukagakusho, the Max Planck Society, and the Higher Education Funding Council for England. The SDSS Web Site is http://www.sdss.org/.

The SDSS is managed by the Astrophysical Research Consortium for the Participating Institutions. The Participating Institutions are the American Museum of Natural History, Astrophysical Institute Potsdam, University of Basel, Cambridge University, Case Western Reserve University, University of Chicago, Drexel University, Fermilab, the Institute for Advanced Study, the Japan Participation Group, Johns Hopkins University, the Joint Institute for Nuclear Astrophysics, the Kavli Institute for Particle Astrophysics and Cosmology, the Korean Scientist Group, the Chinese Academy of Sciences (LAMOST), Los Alamos National Laboratory, the Max-Planck-Institute for Astronomy (MPIA), the Max-Planck-Institute for Astrophysics (MPA), New Mexico State University, Ohio State University, University of Pittsburgh, University of Portsmouth, Princeton University, the United States Naval Observatory, and the University of Washington.

REFERENCES

Adelman-McCarthy, J., et al. 2006, ApJS, 162, 38

Agüeros, M.A. et al. 2006, AJ, 131, 1740

Anderson, S.F., et al. 2003, AJ, 126, 2209 (Paper 1)

Avni, Y., & Tananbaum, H. 1986, ApJ 305, 83

Bade, N., Beckmann, V., Douglas, N.G., Barthel, P.D., Engels, D., Cordis, L., Nass, P., & Voges, W. 1998b, A&A, 334, 459

Bade, N., et al. 1998a, A&AS, 127, 145

Baldwin, J.A., Phillips, M.M., & Terlevich, R. 1981, PASP, 93, 5

Becker, R.H., White, R.L., & Helfand, D.J. 1995, ApJ, 450, 559

Blanton, M.R., Lupton, R.H., Maley, F.M., Young, N., Zehavi, I., & Loveday, J. 2003, AJ, 125, 2276

Boller, Th. 2000, New Astr Rev, 44, 387

Collinge, M.J., et al. 2005, AJ, 129, 2542

Condon, J.J., Cotton, W. D., Greisen, E. W., Yin, Q.F., Perley, R.A., Taylor, G.B., & Broderick, J.J. 1998, AJ, 115, 1693

Dressler, A., & Schectman, S. 1987, AJ, 94, 899

Flesch, E., & Hardcastle, M.J. 2004, A&A, 427, 387

Fukugita, M., Ichikawa, T., Gunn, J.E., Doi, M., Shimasaku, K., & Schneider, D.P. 1996, AJ, 111, 1748

Gallagher, S.C., Brandt, W.N., Chartas, G., & Garmire, G.P. 2002, ApJ, 567, 37

Gioia, I. M., Maccacaro, T., Schild, R. E., Stocke, J. T., Liebert, J. W., Danziger, I. J., Kunth, D., & Lub, J. 1984, ApJ, 283, 495

Green, P.J., Aldcroft, T.L., Mathur, S., Wilkes, B.J., & Elvis, M. 2001, ApJ, 558, 109

Green, P.J., et al. 1995, ApJ, 450, 51

Gunn, J.E., et al. 1998, AJ, 116, 3040

Gunn, J.E., et al. 2006, AJ, 131, 2332

Halpern, J.P., Turner, T.J., & George, I.M. 1999, MNRAS, 307, L47

Hall, P.B., et al. 2002, ApJS, 141, 267

Hao, L., et al. 2005, AJ, 129, 1795

Hogg, D.W., Finkbeiner, D.P., Schlegel, D.J., & Gunn, J.E. 2001, AJ, 122, 2129

Ivezić, Z., et al. 2004, AN, 325, 583

Kewley, L.J., Dopita, M.A., Sutherland, R.S., Heisler, C.A., & Trevena, J. 2001, ApJ, 556, 121

Komossa, S., Voges, W., Adorf, H.-A., Xu, D., Mathur, S., & Anderson, S.F. 2006, ApJ, 639, 710

Körding, E.G., Jester, S., & Fender, R. 2006, MNRAS, submitted

Landt, H., Padovani, P., & Giommi, P. 2002, MNRAS, 336, 945

Laurent-Muehleisen, S. A., Kollgaard, R. I., Ryan, P. J., Feigelson, E. D., Brinkmann, W., & Siebert, J. 1997, A&AS, 122, 235

Lupton, R.H., Gunn, J.E., & Szalay, A. 1999, AJ, 118, 1406

Marchã, M.J.M., Browne, I.W.A., Impey, C.D., & Smith, P.S. 1996, MNRAS, 281, 425

Mickaelian, A.M., Hovhannisyan, L.R., Engels, D., Hagen, H.-J., & Voges, W. 2006, A&A, 449, 425

Morris, S. L., Stocke, J. T., Gioia, I., Schild, R. E., Wolter, A., Maccacaro, T., & della Ceca, R. 1991, ApJ, 380, 49

Perlman, E. S., et al. 1996, ApJS, 104, 251

Pfeffermann, E., Briel, U.G., Hippmann H., et al. 1988, Proc. SPIE, 733, 519

Pier, J.R., Munn, J.A., Hindsley, R.B., Hennessy, G.S., Kent, S.M., Lupton, R.H., & Ivezíc, Z. 2003, AJ, 125, 1559

Pogge, R.W. 2000, New Astr Rev, 44, 381

Richards, G.T., et al. 2002, AJ, 123, 2945

Schartel, N., et al. 1996, MNRAS, 283, 1015

Schlegel, D.J., Finkbeiner, D.P., & Davis, M. 1998, ApJ, 500, 525

Schneider, D.P., et al. 2005, AJ, 130, 367

Shen, S., White, S.D.M., Mo, H.J., Voges, W., Kauffmann, C., & Anderson, S.F. 2006, MNRAS, 369, 1639

Smith, J.A., et al. 2002, AJ, 123, 2121

Stark, A. A., Gammie, C. F., Wilson, R. W., Bally, J., Linke, R. A., Heiles, C., & Hurwitz, M. 1992, ApJS, 79, 7

Steffen A.T., Strateva, I., Brandt, W.N., Alexander, D.M., Koekemoer, A.M., Lehmer, B.D., Schneider, D.P., & Vignali, C. 2006, AJ, 131, 2826

Stocke, J. T., et al. 1991, ApJS, 76, 813

Stoughton, C. et al. 2002, AJ, 123, 485

Strateva, I.V., et al. 2003, AJ, 126, 1720

Trump, J., et al. 2006, ApJS, 165, 1

Tucker, D., et al. 2006, AN, in press

Urry, C. M., & Padovani, P. 1995, PASP 107, 803

Vanden Berk, D.E., et al. 2005, AJ, 129, 2047

Veron-Cetty, M.P., & Veron, P. 2006, VizieR Online Data Catalog, 7248, 0

Vignali, C., Brandt, W.N., & Schneider, D.P. 2003, AJ, 125, 433

Voges, W., et al. 1999, A&A, 349, 389

Voges, W., et al. 2000, IAUC 6420

Weymann, R.J., Morris, S.L., Foltz, C.B., & Hewett, P.C. 1991, ApJ, 373, 23

Wilkes, B.J., Tananbaum, H., Worrall, D. M., Avni, Y., Oey, M. S., & Flanagan, J. 1994, ApJS, 92, 53

Williams, R.J., Pogge, R.W., & Mathur, S. 2002, AJ, 124, 3042

York, D.G., et al. 2000, AJ, 120, 1579

Yuan, W., Brinkmann, W., Siebert, J., & Voges, W. 1998a, A&A, 330, 108

Yuan, W., Siebert, J., & Brinkmann, W. 1998b, A&A, 334, 498

Zakamska, N.L., et al. 2003, AJ, 126, 2125

Zickgraf, F.-J., Engels, D., Hagen, H.-J., Reimers, D., & Voges, W. 2003, A&A, 406, 535

This preprint was prepared with the AAS LaTeX macros v5.2.

Table 1: Observed Parameters of Broad-Line RASS/SDSS AGN[a]

RASS X-ray source RXS J	SDSS optical counterpart SDSS J	u	g	r	i	z	opt morph	red-shift	X-ray count rate	X exp tim	X HR1	X HR2	X like	$f_x \times 10^{13}$
(1)	(2)	(3)	(4)	(5)	(6)	(7)	(8)	(9)	(10)	(11)	(12)	(13)	(14)	(15)
000011.9+000223	000011.96+000225.3	18.24	17.97	18.02	17.96	17.91	6	0.479	0.0219	364	-0.01	-1.00	9	2.20
000024.1+152026	000024.02+152005.4	19.41	19.18	18.99	19.08	19.13	6	0.989	0.0133	463	-0.05	-1.00	8	1.41
000100.8−102318	000102.18−102326.9	18.98	18.69	18.33	18.24	17.66	6	0.294	0.0284	340	0.37	-0.13	8	2.76
000117.2+141150	000116.00+141123.0	19.01	18.68	18.70	18.56	18.16	6	0.404	0.0155	405	1.00	0.14	8	1.74
000133.1+145601	000132.83+145608.0	19.22	19.20	19.25	19.04	18.39	3	0.399	0.0388	473	0.18	-0.86	21	4.28

[a] [The complete version of this table is in the electronic edition of the journal. The printed version contains only a sample.]

Table 2: Derived Parameters of Broad-Line RASS/SDSS AGN[a]

RASS X-ray source RXS J	SDSS optical counterpart SDSS J	g_o	red-shift	$f_x^c \times 10^{13}$	$log(L_x)$	$log(l_{opt})$ 2500Å	$log(l_x)$ 2 kev	α_{ox}	comment
(1)	(2)	(3)	(4)	(5)	(6)	(7)	(8)	(9)	(10)
000011.9+000223	000011.96+000225.3	17.85	0.479	5.42	44.76	30.14	26.22	1.50	LBQS 2357-0014
000024.1+152026	000024.02+152005.4	19.02	0.989	3.60	45.41	30.37	26.88	1.34	...
000100.8−102318	000102.18−102326.9	18.53	0.294	6.60	44.32	29.40	25.78	1.39	...
000117.2+141150	000116.00+141123.0	18.46	0.404	4.68	44.51	29.73	25.97	1.44	...
000133.1+145601	000132.83+145608.0	19.03	0.399	11.36	44.88	29.49	26.34	1.21	...

[a][The complete version of this table is in the electronic edition of the journal. The printed version contains only a sample.]

Table 3: Observed Parameters of RASS/SDSS AGN Having Narrower Permitted Emission[a]

RASS X-ray source RXS J	SDSS optical counterpart SDSS J	u	g	r	i	z	opt morph	red-shift	X-ray count rate	X exp tim	X HR1	X HR2	X like	$f_x \times 10^{13}$
(1)	(2)	(3)	(4)	(5)	(6)	(7)	(8)	(9)	(10)	(11)	(12)	(13)	(14)	(15)
000202.5−103030	000202.95−103038.0	18.06	17.59	17.25	16.81	16.63	3	0.103	0.0610	324	-0.12	-0.14	31	5.94
000250.8+000824	000251.60+000800.7	20.54	19.48	18.67	18.21	17.88	3	0.107	0.0410	388	-0.32	0.09	9	4.10
001056.7−090100	001056.25−090109.9	19.14	18.06	17.57	17.10	16.90	3	0.081	0.0283	343	0.49	1.00	10	2.82
001618.5+011528	001617.83+011522.0	21.06	19.67	18.69	18.18	17.88	3	0.217	0.0398	402	-0.13	-0.14	18	3.78
002608.2−000544	002608.38−000547.0	20.73	19.57	18.81	18.32	17.93	3	0.107	0.0228	415	0.81	0.49	13	2.11

[a] [The complete version of this table is in the electronic edition of the journal. The printed version contains only a sample.]

Table 4: Derived Parameters of RASS/SDSS AGN Having Narrower Permitted Emission[a]

RASS X-ray source RXS J	SDSS optical counterpart SDSS J	g_o	red-shift	$f_x^c \times 10^{13}$	$log(L_x)$	$log(l_{opt})$ 2500Å	$log(l_x)$ 2 kev	α_{ox}	comment
(1)	(2)	(3)	(4)	(5)	(6)	(7)	(8)	(9)	(10)
000202.5−103030	000202.95−103038.0	17.42	0.103	14.25	43.61	28.87	25.07	1.46	Sy1.8,radio
000250.8+000824	000251.60+000800.7	19.35	0.107	10.03	43.49	28.13	24.96	1.22	Sy1.5
001056.7−090100	001056.25−090109.9	17.92	0.081	6.87	43.07	28.45	24.53	1.50	Sy1.8
001618.5+011528	001617.83+011522.0	19.56	0.217	8.89	44.13	28.70	25.60	1.19	Sy1.8
002608.2−000544	002608.38−000547.0	19.48	0.107	4.87	43.18	28.08	24.64	1.32	Sy2?,radio

[a] [The complete version of this table is in the electronic edition of the journal. The printed version contains only a sample.]

Table 5: Observed Parameters of RASS/SDSS BL Lac Candidates[a]

RASS X-ray source RXS J	SDSS optical counterpart SDSS J	u	g	r	i	z	opt morph	red-shift	X-ray count rate	X exp tim	X HR1	X HR2	X like	$f_x \times 10^{13}$
(1)	(2)	(3)	(4)	(5)	(6)	(7)	(8)	(9)	(10)	(11)	(12)	(13)	(14)	(15)
002200.9+000659	002200.95+000657.9	20.48	20.03	19.28	18.87	18.55	3	0.306	0.0973	403	0.08	0.12	55	9.05
003514.9+151513	003514.72+151504.1	17.32	16.93	16.59	16.31	16.05	6	1.090	0.2358	359	0.35	0.25	235	26.95
005041.0−092855	005041.31−092905.1	16.78	16.30	16.03	15.77	15.57	6	...	0.1974	536	0.06	0.16	256	21.34
005620.1−093626	005620.07−093629.8	18.33	17.55	16.96	16.66	16.30	3	0.103	0.3558	335	0.52	0.14	298	38.70
014126.8−092857	014125.83−092843.6	18.11	17.59	17.21	16.97	16.68	6	0.500	0.0344	440	-0.01	0.24	25	3.20

[a] [The complete version of this table is in the electronic edition of the journal. The printed version contains only a sample.]

Table 6: Derived Parameters of RASS/SDSS BL Lac Candidates[a]

RASS X-ray source RXS J	SDSS optical counterpart SDSS J	g_o	red-shift	$f_x^c \times 10^{13}$	$log(L_x)$	$log(l_{opt})$ 2500Å	$log(l_x)$ 2 kev	α_{ox}	comment
(1)	(2)	(3)	(4)	(5)	(6)	(7)	(8)	(9)	(10)
002200.9+000659	002200.95+000657.9	19.94	0.306	21.02	44.86	28.87	26.33	0.98	BL?,radio
003514.9+151513	003514.72+151504.1	16.67	1.090	73.75	46.84	31.41	28.30	1.19	zunc,radio
005041.0−092855	005041.31−092905.1	16.18	...	55.50	...	...	...	1.39	zunc,radio,FBQSJ0050-0929
005620.1−093626	005620.07−093629.8	17.37	0.103	101.2	44.46	28.89	25.92	1.14	BL?,radio,
014126.8−092857	014125.83−092843.6	17.48	0.500	7.42	44.94	30.33	26.41	1.50	zunc,radio,[HB89]0138-097

[a] [The complete version of this table is in the electronic edition of the journal. The printed edition contains only a sample.]